Induction of senescence upon loss of the Ash2l core subunit of H3K4 methyltransferase complexes

Agnieszka Bochyńska [1,†], **Alexander T. Stenzel** [1,†], **Roksaneh Sayadi Boroujeni** [1,†], **Chao-Chung Kuo** [2,3], **Mirna Barsoum** [1], **Weili Liang**[1], **Philip Bussmann**[1], **Ivan G. Costa** [2], **Juliane Lüscher-Firzlaff** [1] **and Bernhard Lüscher** [1,*]

[1]Institute of Biochemistry and Molecular Biology, Faculty of Medicine, RWTH Aachen University, Pauwelsstrasse 30, 52057 Aachen, Germany, [2]Institute for Computational Genomics, Faculty of Medicine, RWTH Aachen University, Pauwelsstrasse 30, 52057 Aachen, Germany and [3]Interdisciplinary Center for Clinical Research (IZKF), Faculty of Medicine, RWTH Aachen University, Aachen, Germany

ABSTRACT

Gene expression is controlled in part by post-translational modifications of core histones. Methylation of lysine 4 of histone H3 (H3K4), associated with open chromatin and gene transcription, is catalyzed by type 2 lysine methyltransferase complexes that require WDR5, RBBP5, ASH2L and DPY30 as core subunits. Ash2l is essential during embryogenesis and for maintaining adult tissues. To expand on the mechanistic understanding of Ash2l, we generated mouse embryo fibroblasts (MEFs) with conditional *Ash2l* alleles. Upon loss of Ash2l, methylation of H3K4 and gene expression were downregulated, which correlated with inhibition of proliferation and cell cycle progression. Moreover, we observed induction of senescence concomitant with a set of downregulated signature genes but independent of SASP. Many of the signature genes are FoxM1 responsive. Indeed, exogenous FOXM1 was sufficient to delay senescence. Thus, although the loss of Ash2l in MEFs has broad and complex consequences, a distinct set of downregulated genes promotes senescence.

INTRODUCTION

The regulated expression of defined genes is important for the identity and physiology of cells. Transcription of genes is regulated by sequence specific transcription factors and by cofactors that control chromatin accessibility and polymerase activity. The smallest units of chromatin are the nucleosomes, which are composed of eight core histones, two copies each of H2A, H2B, H3 and H4 or various variants thereof. Several hundred post-translational modifications (PTM) of core histones have been described, which are thought to regulate specific aspects of transcription (1–3). Methylation of histone H3 at lysine 4 has gained attention because its mono- and tri-methylation (H3K4me1/3) is associated with active enhancers and promoters, respectively. This PTM is catalyzed primarily by lysine-specific methyltransferases of the KMT2 family, consisting of MLL1 to 4, and SET1A and B (KMT2A–D, F and G, respectively). These enzymes are part of multi-subunit complexes, referred to as COMPASS (complex of proteins associated with Set1). All six KMT2 family members associate with the WRAD core complex composed of WDR5, RBBP5, ASH2L and two copies of DPY30, forming functional KMT2 complexes. WRAD is necessary for catalytic activity of KMT2 enzymes. Additional subunits interact specifically with distinct KMT2 complexes, further increasing the diversity and functionality of these methyltransferases (4–9).

The importance of KMT2 complexes is highlighted by many functional studies. All KMT2 complex subunits, which have been knocked-out, are essential in mice (7,8). This is true for the six enzymatic subunits, which are required during defined developmental processes, indicating at least in part distinct functions. Moreover, the two WRAD core complex subunits, Ash2l and Dpy30, are necessary for organismal development and cell proliferation and differentiation in the mouse (10–14). Of note is also that mutations in the *Drosophila melanogaster* orthologue *Ash2* cause homeotic transformations, similar to mutations in *trithorax*, the orthologue of *MLL1* and *MLL2* (15–17). Moreover, KMT2 complex subunits are linked to various diseases, including cancer (7,18). Together, KMT2 complexes/COMPASS contribute to the control of cell proliferation and differentiation and participate in cell fate decisions.

We identified ASH2L as an interaction partner of the oncoprotein c-MYC and our findings suggest that ASH2L has oncogenic activity (19,20). In mice, the loss of Ash2l led to disintegration of hepatocytes (14). In hematopoietic stem and progenitor cells (HSPCs), the knockout of *Ash2l* resulted in an accumulation of cells in a G2/M cell cycle arrest, accompanied with a proliferation and differentiation stop, that resulted in a loss of mature cells (13,14). We have now addressed the function of Ash2l in mouse embryo fibroblasts (MEFs). Unlike the findings in hepatocytes and HSPCs, Ash2l loss in MEFs resulted in a senescence phenotype once cells ceased to proliferate. Senescence is a heterogenous response of cells to a broad spectrum of triggers, which include replicative exhaustion with telomer erosion, oncogene activation, and DNA damage as well as other forms of stress that result in the upregulation of many genes, including those expressing cyclin-dependent kinase inhibitors (21,22). Ash2l loss was accompanied by an overall reduction in gene expression. A small set of downregulated genes are linked to senescence that are also repressed in other senescent cells. Many of these genes are controlled by the transcription factor FoxM1. Its exogenous expression was sufficient to delay senescence. Thus, MEF cells respond to Ash2l loss with a senescence program that depends on downregulation of genes associated with the cell cycle, replication and DNA repair, which is in contrast to the typically observed upregulation of genes.

MATERIALS AND METHODS

Embryonic fibroblasts

Primary fibroblast cultures from littermate embryos (d.p.c. 13.5) were prepared using mice harboring wild-type or exon 4-floxed alleles of *Ash2l* (14) and a single copy of the constitutively expressed transgene CAGGCre-ER^{TM} (strain 004682, The Jackson Laboratory) comprising a fusion between Cre recombinase and the G525R mutant of the mouse estrogen receptor (pMEF, WT: *Ash2l$^{+/+}$/Cre-ER* and KO: *Ash2l$^{fl/fl}$/Cre-ER*). For the generation of immortalized fibroblast cultures (iMEF) the cells were infected with a retrovirus encoding an shRNA against p19^{Arf} (23,24) and a Blasticidin resistance gene used for the initial selection of infected cells (10 μg/ml Blasticidin, Invivogen, ant-bl). MEF cells were cultivated in DMEM (Thermo Fisher Scientific, 61965059) supplemented with 10% heat-inactivated fetal bovine serum (FBS, Thermo Fisher Scientific, 10270106) and 1% penicillin/streptomycin (Thermo Fisher Scientific, 15070063).

KO2 cells of an early passage were infected with lentiviruses expressing HMGB2-eYFP or FOXM1-eYFP fusion proteins and selected with 20 μg/ml hygromycin B (Goldbio Biotechnology, H-270-1). Pools of cells were then cultured in the presence of hygromycin. The expression of FOXM1-eYFP and HMGB2-eYFP was induced by adding 1 μg/ml doxycycline (Sigma Aldrich, D9891).

Induction of recombination

At day 0 cells were treated with 5 nM 4-hydroxytamoxifen (+HOT) (Tocris, 3412) or with vehicle (−HOT, 100% ethanol). Thereafter cells were passaged when needed to maintain subconfluency or solely supplied with new medium with the addition of HOT or vehicle as before.

End-point PCR of genomic DNA

Genomic DNA was isolated using the High Pure PCR Template Preparation Kit (Roche, 11796828001) and the PCR performed using the ALLin Red Taq MasterMix (highQu, PCM0201) according to the manufacturers' instructions. Fragments were analyzed by agarose gel electrophoresis.

RT-qPCR

Total RNA was isolated with the High Pure RNA Isolation Kit (Roche, 11828665001) and cDNA synthesized with the QuantiTect Reverse Transcription Kit (Qiagen, 205314). A SYBR Green reaction mix (QuantiNova, Qiagen 208054) was employed for the quantitative PCR (qPCR) analyses in a RotorGene 6000 cycler (Corbett/Qiagen). For the individual transcripts, QuantiTect Primer Assays (Qiagen) or primers designed with the Primer3 software (http://primer3.ut.ee) were employed as indicated (see Table 1). The efficiency of all primers used was higher than 95%. The PCR reactions were performed with an initial step at 95°C for 2 min, followed by 40 cycles at 95°C for 10 s, 60°C for 10 s, and 72°C for 5 s and a melting curve analysis. Fold changes in expression were calculated according to Pfaffl (25) taking into account the respective primer reaction efficiencies and using *β-glucuronidase* (*Gusb*) as the reference gene as its expression was only little or not affected by the HOT treatment.

RNA-seq

From parallel cell cultures the number of cells was determined and RNA purified as noted above. The cell number was used to adjust the amount of ERCC RNA Spike-In Mix (ThermoFisher Scientific, 4456740). Generation of RNA-seq libraries (TruSeq Stranded Total RNA Sample Library Prep, Illumina, 20020596) and next-generation sequencing (NextSeq 500/550 High Output Kit v2.5, 150 cycles, Illumina, 20024907) were performed by the Genomics Core Facility of the Interdisciplinary Center for Clinical Research (IZKF) Aachen of the Faculty of Medicine at RWTH Aachen University.

Western Blots

Cells were lysed on ice in RIPA buffer (10 mM Tris/HCl, pH 7.4, 150 mM NaCl, 1% Nonidet P-40, 1% deoxycholic acid, 0.1% SDS, protease inhibitor cocktail (1xPIC, Merck, P8340)), containing 10 mM sodium butyrate. After sonication and centrifugation, the protein contents of the supernatants were determined prior to SDS-PAGE and immunoblotting. To verify equal loading the membranes were reversibly stained with 0.2% Ponceau S. The antibodies were applied in 5% low-fat milk, 0.05% Tween20 in PBS. For analyzing p38 phosphorylation, the lysis buffer contained additionally a phosphatase inhibitor cocktail (1 mM orthovanadate, 50 nM okadaic acid, 50 nM β-phospho-glycerol, 25 mM NaF, 5 mM EGTA). The antibodies were applied in

Table 1. Oligonucleotides

Primer name	Sequence (5′-3′)	Function
Exon4 Ash2l_for	CCGCTGACACCTTTGGAATA	To Monitor the loss of exon 4 of *Ash2l* from RNA
Exon4 Ash2l_rev	TTGCTTCCGGAGAAAGTAGG	
P1	AGGCGCATAACGATACCACGAT	To monitor the loss of exon 4 of *Ash2l* from genomic DNA
P2	CCACAACGGGTTCTTCTGTT	
shRNA p19Arf	GAGGGTTTTCTTGGTGAAG	Insert of retrovirus for the repression of p19^{Arf}
RT-qPCR primers		
Mm_Gusb_1_SG	(QT00176715, Qiagen)	Normalizer
Mm_Flywch2_1_SG	(QT00160447, Qiagen)	Monitoring of gene expression
Mm_Cdh3_1_SG	(QT00108878, Qiagen)	
Mm_Tcfl5_1_SG	(QT00153580, Qiagen)	
Mm_Cdh17_1_SG	(QT01055110, Qiagen)	
Mm_Olfr456_1_SG	(QT00362558, Qiagen)	
Mm_Hsp90b1_1_SG	(QT00130522, Qiagen)	
Mm_Il6_1_SG	(QT00098875, Qiagen)	
Mm_Il7_1_SG	(QT00101318, Qiagen)	
Mm_Ccl2_1_SG	(QT00167832, Qiagen)	
Mm_Gstm4_1_SG	(QT00113113, Qiagen)	
Mm_Cntln_1_SG	(QT00147189, Qiagen)	
Mnd1_ChIP_For	GCCATGATCTAAAGGCGGAGTG	Monitoring changes in H3K4me3 at TSS of selected M-Genes
Mnd1_ChIP_Rev	GTTCAGTGCCCTTCGGTTCTC	
Neil3_ChIP_For	GAAACACAGGCTCTAGGTCTTGG	
Neil3_ChIP_Rev	GCAGCGGGAAGTGGAGTAAA	
Pbk_ChIP_For	GGCTTGATTGGCTCGCTTCTA	
Pbk_ChIP_Rev	TGGCTGTGGTCACAGAGGATA	
Ska1_ChIP_For	AAACCTGGAAGCAGTAGTGAGTG	
Ska1_ChIP_Rev	ACAGCCATATTCCCTGTCCTTTC	

5% BSA, 0.05% Tween20 in PBS. The blots were developed with the SuperSignal West Femto Chemiluminescence Substrate (ThermoFisher Scientific, 34094). For details of the antibodies see Table 2.

Monoclonal antibodies recognizing ASH2L were generated as described before (20). Clone 5E10 recognizes an epitope in the N-terminal fragment of ASH2L, which is conserved in the mouse.

In vitro SAM assay

Cell lysates were prepared in Co-IP buffer (10 mM HEPES, pH 7.5, 50 mM NaCl, 30 mM Na$_4$P$_2$O$_7$, 50 mM NaF, 0.2% (v/v) Triton X-100, 10% (v/v) glycerol, 5 μM ZnCl$_2$, 1 × PIC). Lysed cells were mixed vigorously for 45 sec and centrifuged at 16 000 × g and 4°C for 20 min. The protein concentrations of the supernatants were measured and adjusted accordingly. Aliquots were retained for direct Western blot analysis (Input) and otherwise subjected to immunoprecipitation (IP) with protein A-coupled Sepharose beads (Merck, 17-5280-02) pre-incubated with 2 μg anti-RbBP5 antibody or IgG at 4°C for 2 h. Protein–antibody-bead complexes were washed three times with Co-IP buffer and twice with SAM assay buffer (50 mM Tris–HCl (pH 8.0), 5 mM MgCl$_2$, 50 mM NaCl, 1 mM DTT, 1× PIC). Afterwards 2 μg of recombinant human Histone H3.1 (New England BioLabs, M2503), 100 μM S-(5′-adenosyl)-L-methionine chloride dihydrochloride (SAM, Merck, A7007) used as a primary methyl donor molecule, dissolved in 30 μl SAM assay buffer were added to the beads and incubated for 1 h at 31°C with agitation. Subsequently the beads were heated in sample buffer (40 mM Tris pH 6.8, 10% Glycerol, 2% SDS, bromophenol blue) at 95°C for 10 min and used for SDS-PAGE and immunoblotting.

Immunoprecipitation (GFP-Trap)

eYFP-tagged fusion proteins were immunoprecipitated using anti-GFP magnetic agarose beads (Chromotek, gtma-20). After induction of gene expression of lentiviral transduced KO2 cells with 1 μg/ml doxycycline, cells were harvested and pelleted. Lysis was performed with ice cold RIPA buffer as described above. A fraction of the lysate was used as input, while the rest was subjected to IP with 5 μl of magnetic beads. IP samples are incubated on an overhead rotator at 4°C for 2 h and subsequently washed three times in RIPA buffer. The beads were collected in magnetic stand and proteins solubilized in loading buffer as described above.

Chromatin immunoprecipitation

iMEF cells were treated with HOT or vehicle for 5 days and cross-linked with 1% formaldehyde in cell culture medium on a shaking platform for 10 min at room temperature (RT). The cross-linking reaction was quenched by adding glycine to 125 mM and incubation for another 5 min at RT. Adherent cells were washed with cold PBS twice and collected in PBS by scraping the cells from the dish. Cells were centrifuged at 380 × g for 5 min at 4°C and resuspended in 1 ml Lysis Buffer B (10 mM HEPES pH 6.5, 10 mM EDTA, 0.5 M EGTA, 0.25% (v/v) Triton X-100) per 1–2 × 10^7 cells and centrifuged. To the pellet 1 ml Lysis Buffer C (10 mM HEPES pH 6.5, 10 mM EDTA, 0.5 M EGTA, 200 mM NaCl) was added per 1–2 × 10^7 cells, followed by an

Table 2. Antibodies

Antigen	Species	Company/Cat no.	Clonality	RRID number
Primary antibodies (used in western blots)				
Actin	Mouse	MP Biomedicals, 69100, C4	Monoclonal	AB_2335304
Ash2l	Rabbit	Cell Signaling, 5019, D93F6	Monoclonal	AB_1950350
GFP	Goat	Rockland, 600-101-215	Polyclonal	AB_218182
H3K4me3	Rabbit	Abcam, ab8580	Polyclonal	AB_306649
H3K4me2	Rabbit	Abcam, ab7766	Polyclonal	AB_2560996
H3K4me1	Rabbit	Abcam, ab8895	Polyclonal	AB_306847
H3K9me3	Rabbit	Abcam, ab8898	Polyclonal	AB_306848
H3K9ac	Rabbit	Abcam, ab4441	Polyclonal	AB_2118292
H3K27me3	Mouse	Abcam, ab6002	Monoclonal	AB_305237
H3K27ac	Rabbit	Abcam, ab4729	Polyclonal	AB_2118291
H3K79me3	Rabbit	Abcam, ab2621	Polyclonal	AB_303215
H3	Rabbit	Abcam, ab1791	Polyclonal	AB_302613
IgG	Rabbit	Diagenode, C01010080	Polyclonal	AB_2722553
Rbbp5	Rabbit	Bethyl, A300-109A	Polyclonal	AB_210551
Wdr5	Rabbit	Bethyl, A302-429A	Polyclonal	AB_1944302
p38MAPK	Rabbit	Santa Cruz Biotechnology, sc7149	Polyclonal	Antibody no longer available
p38MAPK-P	Rabbit	Cell Signaling, 9211	Polyclonal	AB_331641
γ-H2AX	Mouse	Upstate, Millipore 05–636	Monoclonal	AB_309864
Antbodies (used in ChIP experiments)				
H3K4me3	Rabbit	Abcam, ab8580	Polyclonal	AB_306649
IgG	Rabbit	Diagenode, C01010080	Polyclonal	AB_2722553
Secondary antibodies				
Antigen	**Species**	**Company/Cat no.**	**Conjugation**	
Goat IgG	Mouse	Santa Cruz Biotechnology, sc-2354	HRP-conjugated	
Mouse IgG	Goat	Jackson Immuno Res., 111-035-146	HRP-conjugated	
Rabbit IgG	Goat	Jackson Immuno Res., 111-035-144	HRP-conjugated	
Rat IgG	Goat	Invitrogen, A-11006	Alexa Fluor 488	
Rat IgG	Goat	Invitrogen, A-21434	Alexa Fluor 555	
Rabbit IgG	Goat	Invitrogen, A-21428	Alexa Fluor 555	

incubation on ice for 10 min. After a further centrifugation step, disruption of the pelleted nuclei was performed in 200 µl lysis buffer D (50 mM Tris pH 8, 10 mM EDTA, 1% (w/v) SDS, protease inhibitor cocktail (1× PIC, Merck, P8340) per $0.5–1 \times 10^7$ MEF cells for 30 min at 15°C. 200 µl aliquots were sonicated for a minimum of 5–10 cycles using a Bioruptor Pico (Diagenode) with 30-s on-off-cycles to achieve DNA fragment lengths oscillating around 500 bp for ChIP-qPCR. The size distribution of the resulting DNA fragments was assessed by agarose gel electrophoresis. To remove cell debris, lysates were centrifuged for 10 min at 10 000 × g (15°C), the supernatants pooled, and DNA concentrations were measured using a NanoDrop 1000 device (Peqlab).

The antibodies used are listed in Table 2. ChIP assays were performed using the OneDay ChIP Kit from Diagenode (C01010080) according to the manufacturer's instructions. To capture protein–DNA complexes, 42 µl of Protein A beads per sample were pre-incubated in 1× ChIP buffer for 2 h at 4°C with 2 µg of specific antibody recognizing H3K4me3. For control, an equivalent amount of rabbit IgG was applied. The sheared chromatin (50–70 µg) was diluted 4.7-fold with 1× ChIP buffer, setting aside 1/10 of the diluted chromatin for the input control, and mixed with the pre-incubated beads for 30 min at 4°C. Subsequently, the chromatin-antibody-bead complexes were washed three times with 1× ChIP buffer and taken up in DNA purifying slurry. The diluted input control chromatin was precipitated by the addition of 5 volumes 100% ethanol and centrifuged at 16 000 × g, 4°C for 10 min. The dried pellets were resuspended in RNase-free H_2O and mixed with DNA purifying slurry. The DNA of all samples was reverse crosslinked and further purified according to the manual. Analyses of ChIP-DNA by qPCR were performed in duplicates with diluted 2 µl IP samples and diluted 2 µl input samples. The SYBR Green reaction mix and qPCR program was applied as describe in the section of RT-qPCR. Evaluation of the data was performed by calculating the percent input of the IP samples, taking into account the dilution of the samples.

Immunofluorescence

Immortalized WT and KO iMEF cells were treated with HOT or vehicle for 5 days, fixed in paraformaldehyde (4% in PBS) at RT for 20 min and permeabilized at RT with Triton X100 (0.2% in PBS) for 5 min. Subsequently, unspecific binding sites were blocked with 20% horse serum (HS) in PBS at 37°C for 30 min. All antibodies were applied in 20% HS/PBS: the primary antibody (specific for Ash2l) at 37°C for 45 min and the secondary antibody (anti-rat Alexa Fluor 488) at 37°C for 30 min. On parallel slides primary antibodies (anti-H3K4me3 or anti-γ-H2AX) were incubated overnight at 4°C followed by the secondary antibody (anti-rat or anti-rabbit Alexa Fluor 555) at 37°C for 30 min. After each incubation the cells were washed 3 times with PBS. Finally, the nuclei were visualized with Hoechst 33258 (Merck, B2883, 2 µg/ml in H_2O at RT for 5 min).

Cell proliferation and SA-β-galactosidase staining

To measure the proliferation, pMEF and iMEF cells were seeded in triplicates, treated with HOT or vehicle and

counted at the days indicated using the CASY® Technology Cell Counter (Innovatis) with three measurements per sample.

Staining for senescence-associated β-galactosidase activity (SA-β-Gal) was performed with cells fixed with glutaraldehyde (0.5% in PBS, RT for 10 min) (26–28). After washing twice with PBS containing 2 mM $MgCl_2$ (pH 6.0), the staining solution (5 mM K-ferrocyanide, 5 mM K-ferricyanide, 1 mg/ml X-gal in $MgCl_2$/PBS, pH 6.0) was applied at 37°C overnight. After washing with H_2O, the percentage of blue cells versus the total number of cells was determined.

The senolytics Dasitinib (Cayman Chemical, 11498), Quercetin (Cayman Chemical, 10005169), Compound15e (Enzo Life Science, ALX 270–455) and Wortmannin (Merck, 681675) were dissolved in DMSO and added to cultured cells after 5 days of HOT treatment. Wortmannin was re-added daily.

Flow cytometry analyses

Cell cycle distribution of iMEF cells was analyzed using flow cytometry using the Foxp3/Transcription Factor Staining Buffer Set (eBioscience, 00-5523) according to the manufacturer's instructions. After trypsinization, cell pellets were resuspended in 200 μl PBS and 800 μl of Fixation/Permeabilization Buffer under constant vortexing. After incubation at RT for 15 min, 2 ml of Permeabilisation Buffer was added and the cells were centrifuged with 380 × g at RT for 3 min. For cell cycle distribution the fixed cells were resuspended in Hoechst 33258 (Merck, B2883 1 μg/ml H2O). For nocodazole treatment, the iMEF cells were incubated for 7 days with HOT or vehicle and with 100 ng/ml nocodazole (Merck, M1404) in DMSO or with vehicle for 18 h before sample collection. Apoptosis was assessed using the FITC Annexin V Apoptosis Detection Kit and with propidium iodide staining (Immunostep, ANXVKF) according to the manufacturer's protocol. Measurements were performed using a FACSCanto II system (BD Biosciences) and analyzed with FlowJo software or Flowing Software 2.

Quantification and statistical analysis

Error bars represent standard deviation (SD) of the mean, unless otherwise indicated. Statistical significance was evaluated by multiple *t*-test using GraphPadPrism software, unless otherwise indicated.

Bioinformatics

For RNA-seq, we trimmed sequences using Trim Galore (http://www.bioinformatics.babraham.ac.uk/projects/trim_galore/). The sequences were aligned against the reference genome (UCSC mm9) using STAR for RNA-seq (29). We used Gencode/ENSEMBL annotation (Mouse Release M1) to build a gene count matrix with featureCounts (30). Next, we used DEseq2 (31) to perform differential expression analysis. Genes were normalized only by ERCC (External RNA Controls Consortium) counts. Differentially regulated genes per each cell type and differential promoters are listed in Supplementary Table S1.

GO term/pathway enrichment analyses were performed using the Metascape interface tool (http://metascape.org/gp/index.html) (32). For the GO analysis in Figure 4, we employed g:Profiler (33).

Sequencing data of the RNA-seq experiments have been deposited in Gene Expression Omnibus with the accession number GSE165458. Included are BigWig files and the result of the differential expression analysis of the RNA-seq data: Differential_Expression_Analysis_KO_Ash2l_result.xlsx.

RESULTS

Ash2l is required for fibroblast cell proliferation

We prepared MEF cells from mouse embryos that contained a floxed *Ash2l* exon 4 and that express a Cre-ER^{TM2} recombinase fusion protein. Primary MEFs (pMEFs), were immortalized using an siRNA expression construct that targets the *p19^{ARF}* mRNA (iMEFs) (23,24). Two pairs of iMEF cells were generated, WT1 and WT2 cells (*Ash2l$^{wt/wt}$:Cre-ER^{TM2}*) and KO1 and KO2 cells (*Ash2l$^{fl/fl}$:Cre-ER^{TM2}*), each pair from 2 embryos of the same mother. Upon treatment with 4-hydroxytamoxifen (HOT), which activates the constitutively expressed recombinase, exon 4 sequences were lost in KO but not in WT cells (Supplementary Figure S1A) and exon 4 containing RNA expression decreased strongly (Figure 1A). This was followed by a decrease of Ash2l in KO2 cells (Figure 1B) and in KO1 and pMEF cells (Supplementary Figure S1B and C), albeit slowly due to the long half-life of Ash2l protein (20). The mRNA from alleles with deleted exon 4 could encode a protein of 135 amino acids (129 encoded by exon 1–3 and 6 by exon 5 in an alternative reading frame). A monoclonal antibodies, 5E10, which recognizes an N-terminal epitop of Ash2l was unable to detect this hypothesized N-terminal fragment (Supplementary Figure S1B). As a result, H3K4 methylation decreased (Figure 1C and Supplementary Figure S1C–E), as expected when one of the core components of KMT2 complexes is lost. Moreover, Rbbp5 containing complexes lost H3K4 methyltransferase activity when isolated from cells without Ash2l (Figure 1D). Rbbp5, a direct interaction partner of Ash2l, was reduced at late time points, while Wdr5 was not (Figure 1 and Supplementary Figure S1). Whether this is the result of altered protein stability or translation has not been analyzed. Because RBBP5 and WDR5 are considerably more abundant than all KMT2 subunits combined in HeLa cells (34), and both Rbbp5 and Wdr5 are easily detected in MEF cells, we consider it unlikely that the loss of one but not the other is simply due to the lack of complex assembly. The loss of Ash2l did not affect RNA expression of the core components *Wdr5*, *Rbbp5* and *Dpy30*, and the different catalytic subunits (Supplementary Figure S1F). Thus, loss of Ash2l prevented H3K4 methylation, consistent with previous studies addressing the role of KMT2 complexes (7,8).

Ash2l loss inhibited MEF proliferation beginning between day 3 and 5 upon HOT treatment and ceased by day 6 (Figure 1E and Supplementary Figure S2A). This correlated with the decrease in Ash2l and in H3K4me3 and me1. Unlike in HSPCs, we did not observe an accumulation in the G2/M phase, rather the distribution of the cells
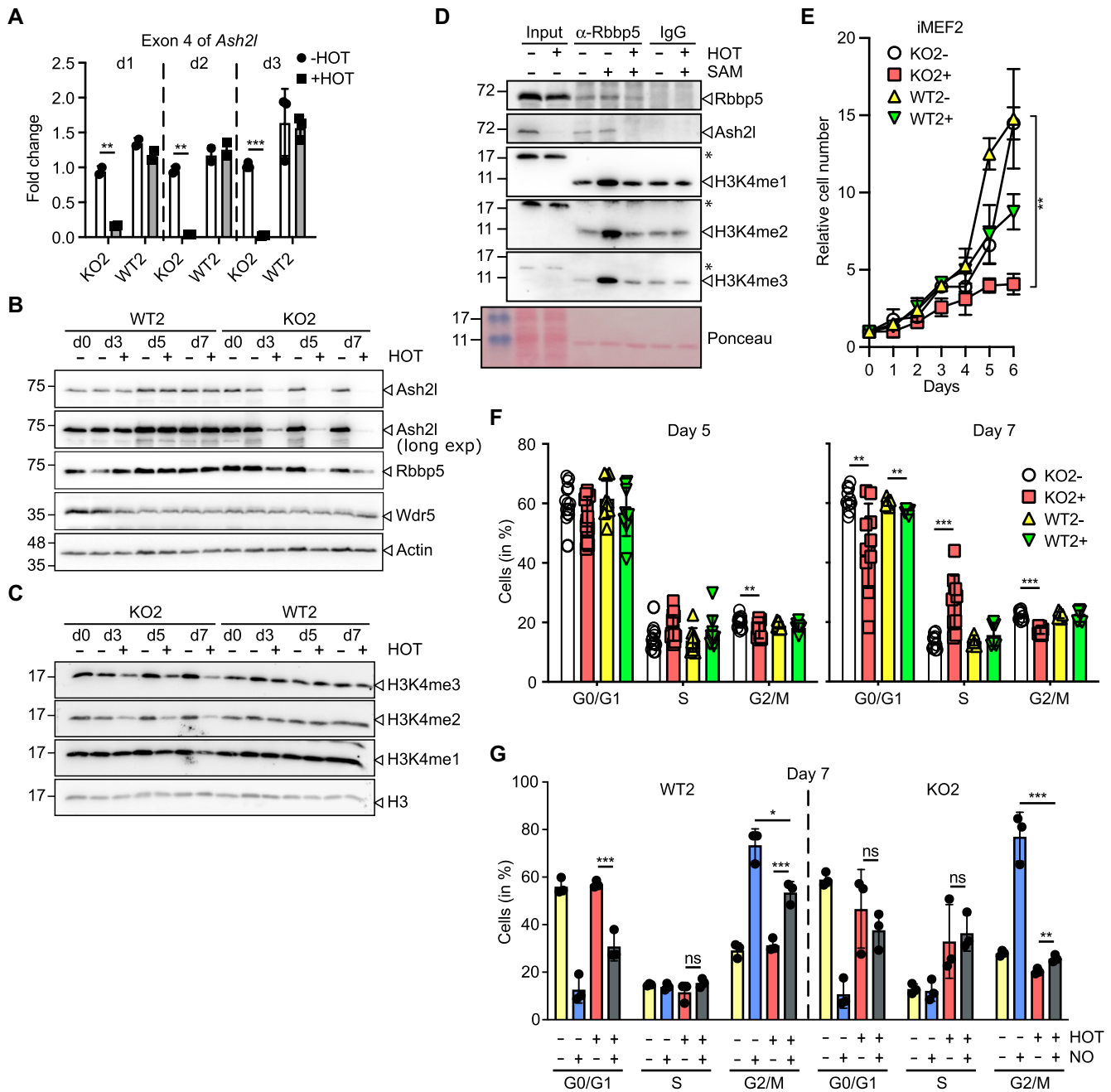
Figure 1. Loss of Ash2l in mouse embryo fibroblasts inhibits proliferation and cell cycle progression. (**A**) iMEF2 cells (WT2, *Ash2l^{wt/wt}:Cre-ER^{TM2}*; and KO2, *Ash2l^{fl/fl}:Cre-ER^{TM2}*) were treated with 4-hydroxytamoxifen (HOT, 5 nM) or vehicle as indicated. RT-qPCR analysis of the floxed exon 4 of *Ash2l* was performed at days 1, 2 and 3. Indicated are mean values ± SD (*** $P < 0.001$; ** $P < 0.01$). (**B, C**) Wild type (WT1) and *Ash2l^{fl/fl}* (KO1) immortalized fibroblasts (iMEF1) were treated ± HOT for 0, 3, 5 or 7 days. The cells were lysed and the indicated proteins analyzed by western blotting. (**D**) KO2 cells were treated ± HOT for 5 days. KMT2 complexes were immunoprecipitated from low stringency lysates using an antibody specific for Rbbp5 or a species matched control antibody (IgG). The immunoprecipitates were incubated in the presence or absence of S-adenosyl-methionine (SAM) and recombinant histone H3. The reactions were analyzed for the proteins indicated using Western blotting. In the input non-specific signals are labeled (*). (**E**) Wild type (WT) and *Ash2l^{fl/fl}* (KO) immortalized fibroblasts (iMEF2) were treated ± HOT (5 nM) for the times indicated. The cells were counted daily. Mean values ± SD of 4–6 measurements in duplicates for each time point (statistical analyses refer to day 6: ** < 0.01). (**F**) Cell cycle analysis using flow cytometry of fixed and Hoechst stained WT2 and KO2 cells treated ± HOT for 5 or 7 days. Mean values ± SD ($n = 6$–10; ** < 0.01, *** < 0.001). (**G**) WT2 and KO2 cells were treated ± HOT for 7 days. During the last 18 h the cells were incubated with nocodazole (100 ng/ml) or vehicle control as indicated. The cells were fixed, the DNA stained using Hoechst and analyzed by flow cytometry. Mean values ± SD of 3 experiments are shown. Statistical analyses are indicated for selected data sets, * <0.05, ** < 0.01, *** < 0.001, ns, not significant.
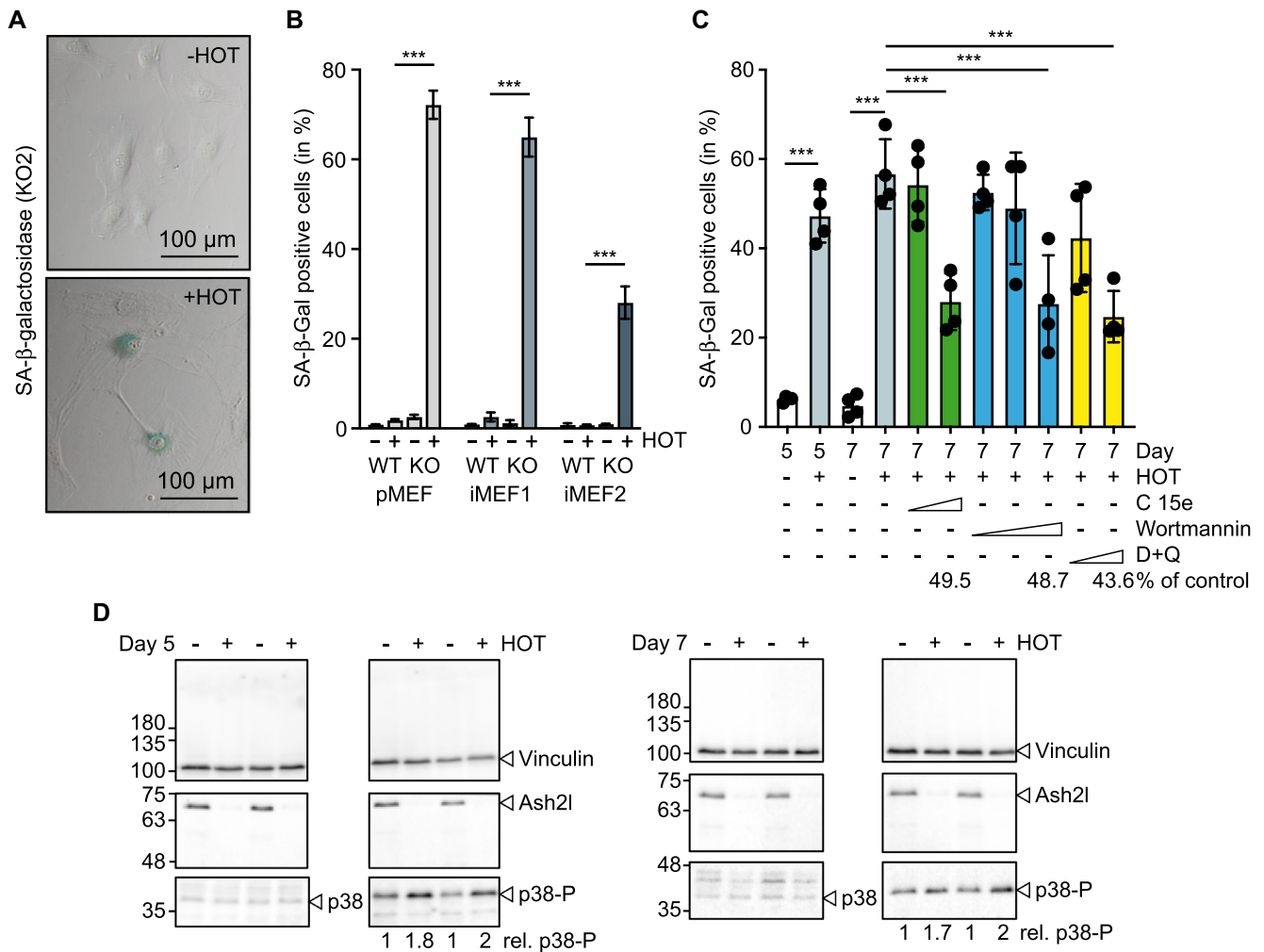
Figure 2. Ash2l loss promotes senescence in MEF cells. (**A**) KO2 cells were incubated ± HOT for 7 days. The cells were fixed and stained for SA-β-galactosidase activity (blue). (**B**) Primary MEF (pMEF) and iMEF cells were treated ± HOT for 5 days as indicated, analyzed as in panel A and the number of SA-β-gal positive cells determined. Mean values ± SD of 3–4 experiments are shown. In each experiment 200–300 cells were counted (*** < 0.001). (**C**) KO2 cells were incubated ± HOT for 7 days. During the last 2 days senolytic drugs were added: Compound 15e (1 and 5 μM), Wortmannin (0.1, 1 and 10 μM), and a combination of Dasatinib/Quercetin (25 nM/1.5 μM and 250 nM/15 μM). The percentage of SA-β-Gal positive cells is displayed. Four sections each with 50–150 cells of two biological replicates were counted. Mean values ± SD ($n = 4$; *** < 0.001). (**D**) KO2 cells were treated ± HOT for 5 or 7 days as indicated. Whole cell lysates of two biological replicates were analyzed by western blotting using the indicated antibodies. Quantified were p38-P versus p38 signals.

in the different cell cycle phases remained largely unaffected with a small increase in S phase at day 7 (Figure 1F and Supplementary Figure S2B and C). This suggested that the cells were unable to transit the cell cycle upon downregulation of Ash2l. To address whether the cells were stalled in the cell cycle, proliferating iMEFs were treated for 18 h with nocodazole, which arrests cells in early mitosis (35). In the absence of HOT, both WT2 and KO2 cells accumulated in G2/M, concomitant with a decrease in G0/G1 cells (Figure 1G). Similarly, an increase in G2/M phase, albeit smaller, was seen in HOT treated WT2 cells. WT cells proliferated slower upon HOT treatment (Figure 1E and Supplementary Figure S2A), explaining the reduced G2/M accumulation. In the absence of Ash2l, the accumulation of KO2 cells in G2/M was minimal (Figure 1G), indicating that these cells were unable to transit through the cell cycle.

We also considered that the loss of Ash2l induced apoptosis, thereby influencing overall proliferation. We did not notice an increase in sub-G0/G1 cells in flow cytometry (Supplementary Figure S2C). Consistent with this observation, staining cells for annexin V and with propidium iodide (PI) did not reveal significant changes, neither in early (annexin V positive) nor late apoptotic cells (both annexin V and PI positive) (Supplementary Figure S2D and E). Thus, cell death is unlikely to contribute significantly to the reduced cell proliferation.

Loss of Ash2l promotes senescence

We noticed that the cells became larger upon loss of Ash2l, an attribute of senescent cells (Figure 2A). Indeed, many cells became SA-β-galactosidase (SA-β-gal) positive (Figure 2A und B), a frequently used marker for senescence (22).
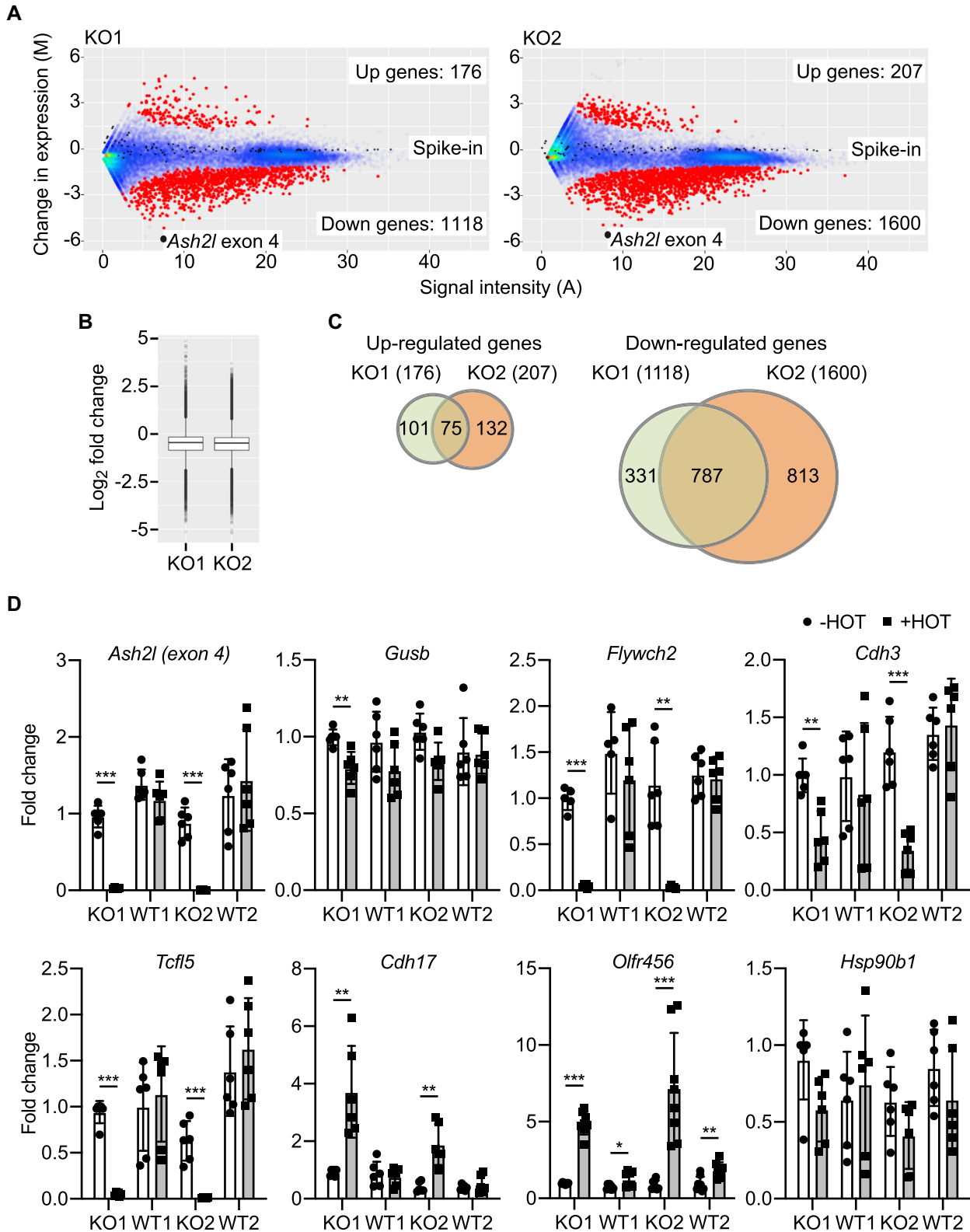
Figure 3. Deregulated gene expression upon loss of Ash2l. (**A**) KO1 and KO2 cells were treated ± HOT for 5 days. RNA was isolated and ERCC RNA spike-in control mix added. The RNA was analyzed using next generation sequencing, adjusted to the spike-in RNA. Displayed are MA plots ($A = 0.5(\log_2(KO + HOT) + \log_2(KO\text{-}HOT))$; $M = \log_2(KO + HOT) - \log_2(KO\text{-}HOT)$). The number of up- and downregulated genes are indicated (*P*-value < 0.05). Red dots, significantly regulated genes; blue dots, not regulated genes; black dots, spike-in RNA. The signals obtained for exon 4 of *Ash2l* are indicated. (**B**) Box plot analysis of gene expression in KO1 and KO2 cells from the data shown in panel A. A one sample t-test indicates that FC values deviate from 0 (*P*-value < 2.2e–16). (**C**) Comparison of up- and downregulated genes between KO1 and KO2 cells. (**D**) WT and KO iMEF1 and 2 cells were incubated ± HOT for 5 days, the RNA isolated and the expression of the indicated genes measured by RT-qPCR. The expression of *Gusb* was used as reference. Mean values ± SD ($n = 5$–8) (* <0.05, ** < 0.01, *** < 0.001).
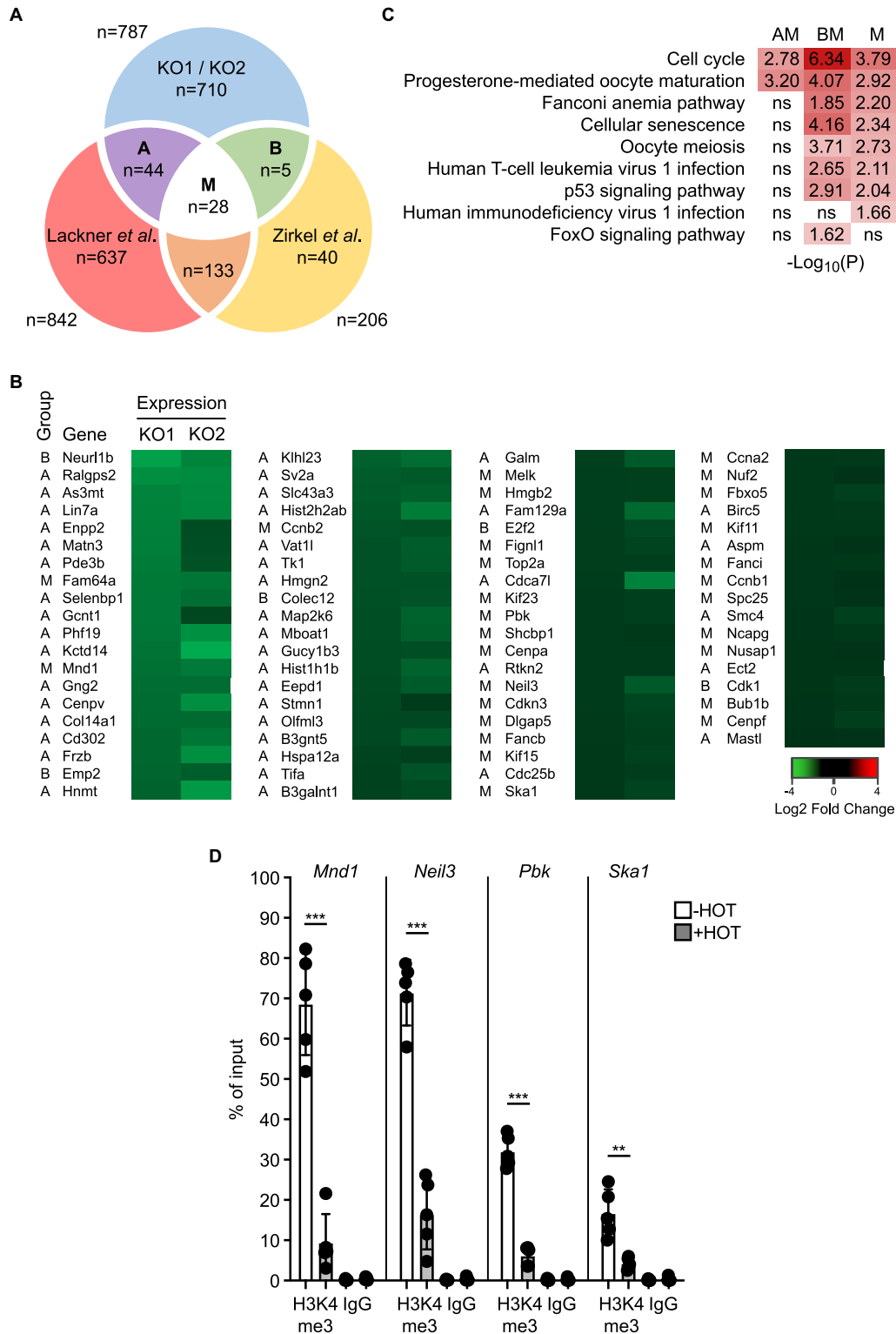
Figure 4. Downregulated genes are associated with the senescence phenotype. (**A**) Commonly downregulated genes in murine KO1 and KO2 cells upon loss of Ash2l were compared to commonly downregulated genes in three primary human cell populations (45) and to downregulated genes in human diploid fibroblasts (44) in response to replicative senescence. The number of genes is indicated that are in common between the different groups: A, KO1/KO2 and the genes in Lackner *et al.*; B, KO1/KO2 and the genes in Zirkel *et al.*; M, common genes of all three studies. Comparison KO1/KO2 with Lackner *et al.* and Zirkel *et al.*: *P*-value < 2.2e–16 (Fischer Exact test). (**B**) The genes in groups A, B and M are listed and the repression of these genes in both KO1 and KO2 cells upon treatment ± HOT for 5 days is indicated. (**C**) GO pathway analysis of the genes that are in common between the data sets of panel A. Adjusted *P*-values are indicated; ns, not significant. (**D**) KO2 cells were treated ± HOT for 5 days. H3K4me3 ChIP-qPCR experiments were performed with primers specific for the promoters of the indicated genes, which belong to the M group (panels A and B). For control, ChIP was carried out using IgG control antibodies. Displayed are mean values ± SD ($n = 5$) (** < 0.01, *** < 0.001).

This phenotype was further assessed by applying senolytic drugs. These have been described to selectively kill senescent cells (36). For example, the combination of Dasatinib and Quercetin eliminated senescent MEFs (37). We observed a reduction of more than 50% of SA-β-gal positive cells with 250 nM Dasatinib/15 μM Quercetin and a trend to less senescent cells with 25 nM Dasatinib/15 μM Quercetin (Figure 2C), while 10 μM Dasatinib/15 μM Quercetin, the originally described dose for MEFs (37), efficiently killed all our cells. Moreover, it was noted that the knockdown of phosphoinositide 3 kinase delta (PI3Kδ) resulted in a senolytic effect (38). Inhibiting PI3 kinases with Wortmannin or compound 15e reduced the number of senescent cells (Figure 2C) (39,40). One of the signaling pathways that is activated during senescence involves p38MAPK, a stress response kinase (41). Indeed, the loss of Ash2l resulted in activating phosphorylation of p38MAPK (Figure 2D). Thus, the loss of Ash2l in MEF cells promotes senescence.

Downregulation of gene expression upon loss of Ash2l

A hallmark of senescent cells is the secretion of signaling and extracellular matrix modulating molecules, at least in part due to an altered gene expression program, referred to as senescence-associated secretory phenotype (SASP) (22,42,43). Because KMT2 complexes are associated with altered gene transcription, we performed RNA-seq experiments to evaluate changes in gene expression, which might account for the senescence phenotype, upon Ash2l loss five days after HOT addition (Supplementary Table S1). In view of the strong correlation of H3K4me1 and me3 with active enhancer and promoters, respectively, we expected broad effects on gene expression and cellular RNA content. To compensate for this, we used ERCC (External RNA Controls Consortium) spike-in RNA. Roughly 75% of all genes (37205) showed reduced expression ($\log_2 FC < 0$) in the HOT treated KO1 and KO2 cells (Figure 3A and B). We observed 1118 and 1600 significantly downregulated genes in KO1 and KO2 cells, respectively (Figure 3A and C). Also, a small number of genes were up-regulated (176 and 207 in KO1 and KO2 cells, respectively) (Figure 3A and C). Of note, all the apparently upregulated genes had very low basal expression (Supplementary Table S1).

Altered gene expression was verified in independent RT-qPCR experiments. *Ash2l* exon 4 expression was strongly decreased as expected (Figure 3A and D). The expression of *β-glucuronidase (Gusb)* was only slightly downregulated, consistent with the trend to decreased expression of many genes, and served as control (Figure 3D). RNA-seq revealed that *Flywch2*, *Tcfl5* and *Cdh3* were downregulated, the former two being in the top group. *Cdh17* and *Olfr456* were up-regulated while the expression of *Hsp90b1* showed little change (Supplementary Table S1). The differential expression of these genes was reproduced in the RT-qPCR experiments (Figure 3D). Thus, the loss of Ash2l resulted in broadly deregulated gene expression.

We employed gene ontology (GO) analyses to evaluate whether the deregulated genes would allow to make predictions about the cellular processes that might be affected upon Ash2l loss, particularly considering a link to senescence. A large number of terms were observed for down-regulated genes (Supplementary Figure S3A), When upregulated genes were analyzed, only four GO terms were statistically significant (Supplementary Figure S3B). The terms were very broad, but included some related to cell cycle and proliferation. Nevertheless, terms that would suggest a direct link to senescence were not observed in either group.

Gene repression is associated with senescence

One of the key events is the induction of SASP that arguably occurs in all senescent cells (22). Because SASP is primarily based on gene induction, it is unlikely that this can be observed in the *Ash2l* KO cells as the major response is gene repression (Figure 3). Therefore, we compared our downregulated genes with those of two studies (44,45). In one senescence was induced in three primary human cell populations, i.e. umbilical vein endothelial cells, fetal lung fibroblasts, and mesenchymal stromal cells, by replicative exhaustion (45). Gene expression was measured when roughly 65% senescent cells had accumulated as determined by SA-β-gal staining. Of the several hundred downregulated genes in each cell population, 206 were in common between the 3 cell populations (45). We found that 37 and 87 homologous genes were significantly downregulated in KO1 and KO2 cells, respectively, despite comparing human and mouse expression patterns. Thirty-three of these genes were downregulated in both KO iMEF populations (Figure 4A and B, B + M genes). In the second study, replicative senescence was analyzed in human diploid fibroblasts (44). Downregulated genes were enriched for pathways associated with proliferation and replication. We observed an overlap of 72 genes with our dataset (Figure 4A and B, A + M genes). Moreover, the genes in the M group are also downregulated in other studies of cellular senescence (46,47). Importantly, GO pathway analyses of these genes (A, B and M) revealed terms associated with cellular senescence (Figure 4C, e.g. cellular senescence, p53 signaling pathway). Consistent with inhibition of proliferation and cell cycle progression were additional terms (Figure 4C, e.g. Faconi anemia pathway, p53 signaling pathway, FoxO signaling pathway) and the repression of many genes associated with the cell cycle and replication (Supplementary Table S2). Also the terms relating to virus infection are consistent with a proliferation stop as cellular response and senescence (Figure 4C) (48). Together, these changes in gene expression render further support for induction of senescence upon Ash2l loss.

Because H3K4me3 correlates with gene expression (8,9), we asked whether H3K4me3 would be altered at promoters of M genes using chromatin immunoprecipitation (ChIP). We selected the promoters of four genes, which are downregulated between 3- and 7-fold. In human systems, two have been suggested to be controlled by FOXM1, *SKA1* and *PBK* (49,50), while the expression of *NEIL3* and *MND1* correlates with *FOXM1* (51,52) (see also below). On all four promoters we observed a strong decrease of H3K4me3 upon Ash2l loss (Figure 4D), supporting the notion that gene repression and reduction of H3K4me3 correlate.

To obtain information about the dynamics of events, e.g. whether a transient SASP response might occur, we performed time course experiments. The first SA-β-gal pos-

itive cells appeared at day 4 (Figure 5A), concomitant with inhibition of cell proliferation (Figure 1E and Supplementary Figure S2A). The loss of Ash2l and the decrease in H3K4 methylation may affect chromatin and provoke transcription-replication conflicts (53), which may result in DNA damage that is known to contribute to induction of senescence (54). Therefore, we measured γ-H2AX, the phosphorylated form of histone H2AX, a marker for double strand DNA breaks (55,56). Occasionally we observed Ash2l negative cells that stained positive for γ-H2AX at day 5 (Supplementary Figure S4A). However, no broad induction of γ-H2AX in response to Ash2l loss was observed prior to significant senescence induction at days 5 and 7 (Supplementary Figure S4A).

Because SASP is a prominent feature of senescent cells, we considered that genes expressing SASP factors might be induced transiently, prior to the appearance of SA-β-gal positive cells. This might occur prior to inhibition of cell proliferation, which we may have missed in our RNA-seq experiments. Therefore, we measured RNA expression over 7 days upon HOT treatment. For control, two downregulated, *Flywch2* and *Cdh3*, and two up-regulated genes, *Cdh17* and *Olfr456*, were measured (Figure 5B). *Flywch2* and *Cdh3* were strongly repressed by day 3 while induction of RNA expression was a late event. This supports the notion that upregulation of genes was most likely an indirect consequence of Ash2l loss. We analyzed three SASP genes, *IL6*, *IL7* and *Ccl2*, that show basal expression in MEF cells and which are typically upregulated in senescent cells (22). All three were initially downregulated. At later time points, parallel to the appearance of SA-β-gal positive cells, *IL6* and *IL7* expression was enhanced (Figure 5B). At present it is unclear how the mRNAs of these genes are upregulated. Additionally, we analyzed two genes, *Gstm4* and *Cntln*, that were identified as downregulated core senescence signature genes in three different cell types, including human foreskin fibroblasts (57). Both were also repressed in our iMEF cells (Figure 5B).

The transcription factor FOXM1 delays senescence induced by Ash2l loss

When the M genes were analyzed, it was obvious that many fulfill functions in the regulation of the cell cycle, in particular the metaphase—anaphase transition, and in DNA repair and genomic stability, consistent with the GO analysis (Figure 4C). Many of the genes in the M group are regulated by the transcription factor FoxM1 (e.g. (49,50,58–60)), some of which antagonize senescence (e.g. (61–63)). Moreover, FoxM1 itself is promoting cell cycle progression, having functional relevance both at the G1-S and the G2-M transitions (e.g. (64–68)). Also, in several cellular systems, the exogenous expression of FoxM1 was sufficient to interfere with induction of senescence (e.g. (69–73)). Moreover, recent findings suggest that downregulation of FoxM1 is important for senescence induction (74). In human fibroblasts, FOXM1 together with subunits of the DREAM complex hampers senescence (75). These studies suggest that FoxM1 has an important function in controlling senescence. High mobility group proteins, including Hmgb2, possess functions in the control of chromatin and its downregulation is

an early marker for senescence and aging (45,76,77). Moreover, HMGB2 is induced when cells enter the cell cycle (78), and HMGB2 interferes with senescence (79). Based on these published findings, we generated iMEF cells in which we introduced inducible expression constructs for FOXM1 and HMGB2, both fused to eYFP, into KO2 cells. Pools of cells were then treated with HOT and the induction of the transgenes induced with doxycycline. The expression of FOXM1 delayed the development of senescent cells, suggesting that FOXM1 and its downstream targets are relevant downregulated genes in the Ash2l model (Figure 5C). Unlike FOXM1, HMGB2, was not affecting senescence, despite its potential broad role in regulating chromatin and gene transcription.

DISCUSSION

We report on the consequences of the loss of Ash2l in MEF cells. Ash2l is necessary for proliferation and cell cycle progression of these cells. The loss of Ash2l does not result in a specific block in the cell cycle but rather cells appear to arrest through all phases. Moreover, we did not observe any cell death, rather the cells developed a flat, senescence-like phenotype. Consistent with senescence, iMEF cells became SA-β-gal positive. This appears to be the consequence of broad downregulation of gene expression. In particular we noticed a set of downregulated genes that are also apparent in other senescent cells. However, no SASP was observed, which is a hallmark broadly detectable in senescent cells. We noticed that many of the downregulated genes, which are linked to cell cycle progression and stress response, are controlled by the transcription factor FOXM1. This factor is important for cell cycle progression, particularly at the G1-S and G2-M transitions. When *Ash2l* was deleted in cells that express exogenous FOXM1, senescence was delayed. Together the findings suggest that downregulation of FOXM1 target genes is part of the circuitry that promotes senescence upon Ash2l loss and broad downregulation of gene transcription.

The loss of Ash2l results in depletion of H3K4 methylation, consistent with the observations that the WRAD core complex is necessary for KMT2 catalytic activity (Figure 1) (80–85). H3K4me1 and H3K4me3 correlate well with active enhancers and promoters, respectively (4,8,9). This is coherent with the observation that most genes are downregulated (Figure 3). A number of suggestions have been made how H3K4 methylation might affect gene transcription. H3K4me3 provides binding sites for cofactors and thus may contribute to the local organization of chromatin (86–90). One of the readers that binds to H3K4me3 is TAF3, a subunit of the TFIID complex and thus intimately associated with Pol II loading onto core promoters (91). TAF3 possesses a PHD finger that recognizes H3K4me3 (92). This interaction is antagonized by asymmetric demethylation of H3 arginine 2 (H3R2me2a), which also affects methylation of neighboring K4 (93). Localizing H3R2me2a suggests that it is excluded from active promoters and thus provides evidence for crosstalk between these two marks. The essential nucleosome remodeling factor NURF can also bind to H3K4me3 and thus may provide local, promoter associated chromatin remodeling activity (94,95). Multiple additional
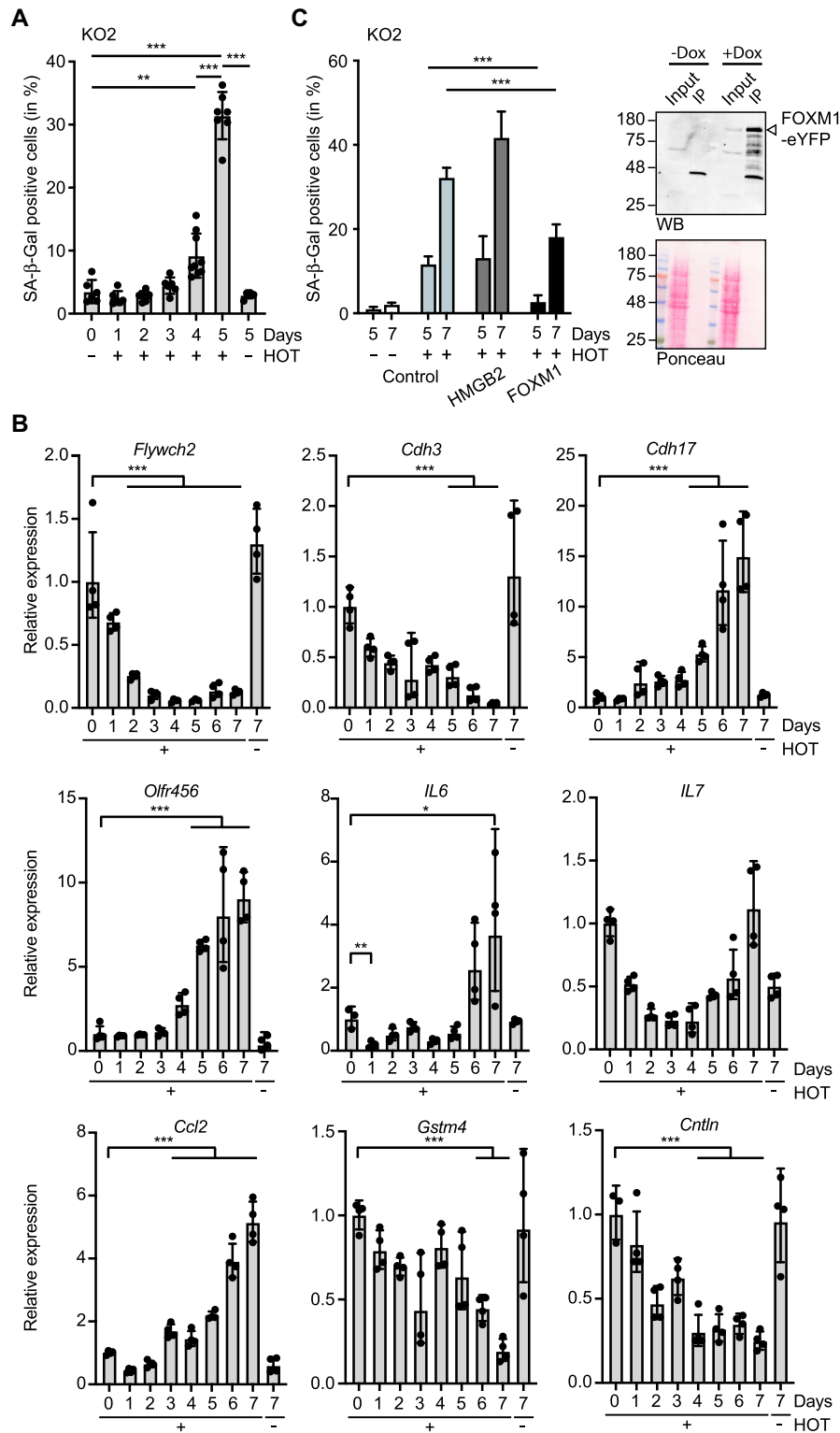
Figure 5. FOXM1 delays Ash2l loss induced senescence. (**A**) KO2 cells were treated with ± HOT for the indicated days. Then cells were fixed and stained for SA-β-galactosidase activity and counted. Mean values ± SD ($n = 6–7$) (*$P < 0.05$, **$P < 0.01$, ***$P < 0.001$). (**B**) KO2 cells were incubated ± HOT for 1–7 days, the RNA isolated and the expression of the indicated genes measured by RT-qPCR. The expression of *Gusb* was used as control. Mean values ± SD ($n = 4$) (*$P < 0.05$, **$P < 0.01$, ***$P < 0.001$). (**C**) KO2 cells were infected with lentiviruses expressing HMGB2 and FOXM1 (as eYFP fusion proteins). Pools of cells were treated with HOT as indicated and with doxycycline (Dox). The number of SA-β-galactosidase positive cells was determined at days 5 and 7. Slides of two biological replicates analyzed in duplicates were blinded and counted by three persons. The resulting mean values ± SD (***$P < 0.001$) are depicted. The panel on the right documents FOXM1-eYFP expression in KO2 cells upon induction with Dox using Western blotting (WB). Input refers to 2.5% of total cell lysate, the remainder was used for immunoprecipitating the fusion protein (IP). Prior to specific protein detection, the membranes were stained with Ponceau S to verify equal loading of input lysates.

factors, including inhibitor of growth (ING) proteins and the chromatin associated factor PHF13/SPOC1, were identified as readers of H3K4me3 that might be associated with gene transcription (5,96,97). Thus, the loss of H3K4 methylation at promoters is likely to have multiple consequences, many are consistent with reduced gene expression.

In hematopoietic cells, the loss of Ash2l resulted in a cell cycle arrest in late G2/early M phase and as a consequence differentiation to mature cells was inhibited (13). Similarly, Dpy30 is necessary for hematopoietic cell proliferation and differentiation. *Dpy30* KO hematopoietic cells also accumulate at the HSPC state (12,98), suggesting that the main phenotype observed upon loss of either Ash2l or Dpy30 is due to the inactivation of KMT2 complexes. However, unlike in HSPCs, the fibroblasts did not accumulate in any particular cell cycle phase, with the exception of a small increase in S phase cells (Figure 1). Among the downregulated genes were many that encode cell cycle regulators, such as different cyclins, Cdk1 and E2F transcription factors (99), and replication factors, including 4 out of 6 minichromosome maintenance proteins (Mcm) (Table S2). The Mcm2–7 complex functions together with additional proteins as essential helicase during DNA double strand opening (100). Thus, the observed cell cycle phenotype is in agreement with the repression of genes that encode essential regulators of both cell cycle progression and replication. We assume that depending on the process that becomes limiting first, cells arrest in different phases of the cell cycle.

The phenotypic outcome of Ash2l loss in iMEF cells is senescence. This is a highly heterogeneous process when comparing different cell types and conditions. Stress-induced irreversible proliferation arrest and resistance to both mitogenic and oncogenic stimuli have been suggested to best define the senescent state (22,43,54). Also the observed cell cycle arrest and the lack of apoptosis are features of senescent cells (101). Typical stressors include excessive replication (replication stress), the induction of oncogenes (oncogene-induced senescence), and DNA damage (e.g. ionizing radiation-induced senescence). These result in both activation and repression of distinct sets of genes. One prominent consequence is the activation of SASP, which has been argued to occur in all senescent cells (22,42,43). SASP genes encode a broad repertoire of different proteins, including cytokines, growth factors and matrix metalloproteinases. These affect the physiology of neighboring cells and are also responsible for many of the pathophysiological consequences as documented for example in cancer (102,103). While genes associated with SASP, such as *Cxcl1*, *Cxcl16* and *IGFBP-6* were slightly upregulated, albeit not significantly (Supplementary Table S1), we did not observe a broad SASP response. *IL6*, *IL7* and *Ccl2*, prominent members of SASP, were initially downregulated upon loss of Ash2l, while at later time points we observed an increase in *Ccl2* by RT-qPCR (Figure 5), while these genes were not affected in RNA-seq (Supplementary Table S1). We interpret this as an attempt to activate SASP as part of the senescence response to downregulation of Ash2l but activation of gene expression is inefficient or not possible once H3K4 methylation is lacking. This is also consistent with the finding that MLL1/KMT2A is essential for SASP (104).

MAP kinases, including p38MAPK, have been described to be important signaling molecules during senescence and to activate SASP (105–108). Indeed, we observed activation of p38MAPK (Figure 2). Moreover, the activation of PI3 kinases has been connected to anti-apoptosis in senescent cells as inhibiting this kinase and downstream effectors are senolytic (37,38,109). Inhibiting MAP kinases by Dasatinib (110) and PI3 kinases by Compound 15e, Wortmannin and Quercetin showed senolytic effects in KO2 cells, consistent with these being senescent upon loss of Ash2l.

A number of reports have indicated that gene repression is also associated with senescence. We compared our down-regulated genes with those that are associated with senescence in a number of different setups in human primary and cancer cells (44–47). We identified a group of 28 genes that were in common (Figure 4). GO analysis identified senescence, cell cycle and stress as relevant terms. Several of the genes in this group encode proteins directly linked to senescence. This includes HMGB2, which is downregulated early in senescence (45), and during aging (77). Conversely, the expression of HMGB2 is induced when cell enter the cell cycle form a quiescent state (78). A role of HMGB2 in senescence is further supported by its role in inhibiting the spreading of heterochromatin, which ensures expression of SASP genes (79). However, the expression of HMGB2 was not sufficient to affect senescence in iMEF cells (Figure 5).

Moreover, Cenpa, Neil3 and cyclin A2 can interfere with senescence (63,111,112). In addition, several other member of the M group seem to affect senescence indirectly. Of particular interest is that many of these genes are regulated by FOXM1, as listed above. Indeed, the expression of FOXM1 in iMEF cells slowed the appearance of senescence cells by 2 days (Figure 5).

Of note is that previous studies have suggested a link of KMT2 complex subunits to senescence. MLL1/KMT2A is frequently translocated in leukemias (113). The MLL1-ENL fusion protein, which promotes aberrant proliferation, provokes a DNA damage response and senescence, initially restricting tumor cell proliferation (114). The knockdown of SET1A/KMT2F, which is frequently overexpressed in tumors, results in mitotic defects and senescence (115). Also, several WRAD subunits are associated with senescence. In rat renal fibroblasts, stress-induced senescence correlates with the expression of p16INK4a, a cell cycle inhibitor associated with oncogene-induced senescence (43). Repression of p16INK4a using inhibitors that interfere with the interaction of Mll1 with the WRAD subunit Wdr5 prevented senescence (116). Moreover, the knockdown of DPY30 in human fibroblasts induces senescence. As in the renal fibroblasts, this was accompanied with an increase in p16INK4a expression (117). Mechanistically, reduced DPY30 results in decreased expression of *ID* genes. ID proteins interfere with ETS transcription factors, which in turn stimulate the expression of the p16INK4a encoding gene *CDKN2A*. Of note, *Cdkn2a* was not induced in our Ash2l KO cells. The difference may be that the Ash2l KO reduces KMT2 complex activities more severely, resulting, as discussed above, in the inability to induce gene expression. Furthermore, DPY30 is a very abundant protein compared to most other KMT2 complex components, in particular the enzymatic subunits (34). Thus, even efficient knock-

down may still leave sufficient DPY30 for KMT2 complex formation and selected gene activation. In summary, we identified the trithorax protein Ash2l as a regulator of senescence in fibroblasts. The *Ash2l* KO MEFs displayed many hallmarks of senescent cells but lacked the typical activation of genes encoding SASP factors. Instead, we find that the downregulation of M group genes provide a signature that seems to be relevant for many different senescent phenotypes.

DATA AVAILABILITY

Sequencing data of the RNA-seq experiments (Suppl. Table S1) have been deposited in Gene Expression Omnibus under accession number GSE165458.

SUPPLEMENTARY DATA

Supplementary Data are available at NAR Online.

ACKNOWLEDGEMENTS

FUNDING

REFERENCES

1. Kornberg,R.D. and Lorch,Y. (2020) Perspective primary role of the nucleosome. *Mol. Cell*, **79**, 371–375.
2. Zhou,K.D., Gaullier,G. and Luger,K. (2019) Nucleosome structure and dynamics are coming of age. *Nat. Struct. Mol. Biol.*, **26**, 3–13.
3. Zentner,G.E. and Henikoff,S. (2013) Regulation of nucleosome dynamics by histone modifications. *Nat. Struct. Mol. Biol.*, **20**, 259–266.
4. Morgan,M.A.J. and Shilatifard,A. (2020) Reevaluating the roles of histone-modifying enzymes and their associated chromatin modifications in transcriptional regulation. *Nat. Genet.*, **52**, 1271–1281.
5. Bochynska,A., Luscher-Firzlaff,J. and Luscher,B. (2018) Modes of interaction of KMT2 histone H3 Lysine 4 Methyltransferase/COMPASS complexes with chromatin. *Cells*, **7**, 17.
6. Shilatifard,A. (2012) The COMPASS family of histone H3K4 methylases: mechanisms of regulation in development and disease pathogenesis. *Annu. Rev. Biochem.*, **81**, 65–95.
7. Rao,R.C. and Dou,Y. (2015) Hijacked in cancer: the KMT2 (MLL) family of methyltransferases. *Nat. Rev. Cancer*, **15**, 334–346.
8. Jiang,H. (2020) The complex activities of the SET1/MLL complex core subunits in development and disease. *BBA-Gene Regul. Mech.*, **1863**, 194560.
9. Hughes,A.L., Kelley,J.R. and Klose,R.J. (2020) Understanding the interplay between CpG island-associated gene promoters and H3K4 methylation. *Biochim. Biophys. Acta Gene Regul. Mech.*, **1863**, 194567.
10. Stoller,J.Z., Huang,L., Tan,C.C., Huang,F., Zhou,D.D., Yang,J., Gelb,B.D. and Epstein,J.A. (2010) Ash2l interacts with Tbx1 and is required during early embryogenesis. *Exp. Biol. Med. (Maywood)*, **235**, 569–576.
11. Bertero,A., Madrigal,P., Galli,A., Hubner,N.C., Moreno,I., Burks,D., Brown,S., Pedersen,R.A., Gaffney,D., Mendjan,S. *et al.* (2015) Activin/nodal signaling and NANOG orchestrate human embryonic stem cell fate decisions by controlling the H3K4me3 chromatin mark. *Genes Dev.*, **29**, 702–717.
12. Yang,Z., Shah,K., Khodadadi-Jamayran,A. and Jiang,H. (2016) Dpy30 is critical for maintaining the identity and function of adult hematopoietic stem cells. *J. Exp. Med.*, **213**, 2349–2364.
13. Luscher-Firzlaff,J., Chatain,N., Kuo,C.C., Braunschweig,T., Bochynska,A., Ullius,A., Denecke,B., Costa,I.G., Koschmieder,S. and Luscher,B. (2019) Hematopoietic stem and progenitor cell proliferation and differentiation requires the trithorax protein Ash2l. *Sci. Rep.*, **9**, 8262.
14. Liang,W.L., Luscher-Firzlaff,J., Ullius,A., Schneider,U., Longerich,T. and Luscher,B. (2016) Loss of the epigenetic regulator Ash2l results in desintegration of hepatocytes and liver failure. *Int. J. Clin. Exp. Pathol.*, **9**, 5167–5175.
15. Shearn,A. (1989) The ash-1, ash-2 and trithorax genes of Drosophila melanogaster are functionally related. *Genetics*, **121**, 517–525.
16. Shearn,A., Hersperger,E. and Hersperger,G. (1987) Genetic studies of mutations at two loci of Drosophila melanogaster which cause a wide variety of homeotic transformations. *Rouxs Arch. Dev. Biol.*, **196**, 231–242.
17. Ingham,P.W. (1981) Trithorax: a new homoeotic mutation of *Drosophila melanogaster*. II. The role oftrx (+) after embryogenesis. *Wilehm Roux Arch. Dev. Biol.*, **190**, 365–369.
18. Poreba,E., Lesniewicz,K. and Durzynska,J. (2020) Aberrant activity of histone-lysine N-Methyltransferase 2 (KMT2) complexes in oncogenesis. *Int. J. Mol. Sci.*, **21**, 9340.
19. Ullius,A., Luscher-Firzlaff,J., Costa,I.G., Walsemann,G., Forst,A.H., Gusmao,E.G., Kapelle,K., Kleine,H., Kremmer,E., Vervoorts,J. *et al.* (2014) The interaction of MYC with the trithorax protein ASH2L promotes gene transcription by regulating H3K27 modification. *Nucleic Acids Res.*, **42**, 6901–6920.
20. Luscher-Firzlaff,J., Gawlista,I., Vervoorts,J., Kapelle,K., Braunschweig,T., Walsemann,G., Rodgarkia-Schamberger,C., Schuchlautz,H., Dreschers,S., Kremmer,E. *et al.* (2008) The human trithorax protein hASH2 functions as an oncoprotein. *Cancer Res.*, **68**, 749–758.
21. Di Micco,R., Krizhanovsky,V., Baker,D. and d'Adda di Fagagna,F. (2021) Cellular senescence in ageing: from mechanisms to therapeutic opportunities. *Nat. Rev. Mol. Cell Biol.*, **22**, 75–95.
22. Sikora,E., Bielak-Zmijewska,A. and Mosieniak,G. (2021) A common signature of cellular senescence; does it exist?*Ageing Res. Rev.*, **71**, 101458.
23. Carnero,A., Hudson,J.D., Price,C.M. and Beach,D.H. (2000) p16INK4A and p19ARF act in overlapping pathways in cellular immortalization. *Nat. Cell Biol.*, **2**, 148–155.
24. Tzatsos,A., Pfau,R., Kampranis,S.C. and Tsichlis,P.N. (2009) Ndy1/KDM2B immortalizes mouse embryonic fibroblasts by repressing the Ink4a/Arf locus. *Proc. Natl. Acad. Sci. U.S.A.*, **106**, 2641–2646.
25. Pfaffl,M.W. (2001) A new mathematical model for relative quantification in real-time RT-PCR. *Nucleic Acids Res.*, **29**, e45.

26. Dimri,G.P., Lee,X., Basile,G., Acosta,M., Scott,G., Roskelley,C., Medrano,E.E., Linskens,M., Rubelj,I., Pereira-Smith,O. *et al.* (1995) A biomarker that identifies senescent human cells in culture and in aging skin in vivo. *Proc. Natl. Acad. Sci. U.S.A.*, **92**, 9363–9367.

27. Kurz,D.J., Decary,S., Hong,Y. and Erusalimsky,J.D. (2000) Senescence-associated (beta)-galactosidase reflects an increase in lysosomal mass during replicative ageing of human endothelial cells. *J. Cell Sci.*, **113**, 3613–3622.

28. Hydbring,P., Bahram,F., Su,Y., Tronnersjo,S., Hogstrand,K., von der Lehr,N., Sharifi,H.R., Lilischkis,R., Hein,N., Wu,S. *et al.* (2010) Phosphorylation by Cdk2 is required for Myc to repress Ras-induced senescence in cotransformation. *Proc. Natl. Acad. Sci. U.S.A.*, **107**, 58–63.

29. Dobin,A., Davis,C.A., Schlesinger,F., Drenkow,J., Zaleski,C., Jha,S., Batut,P., Chaisson,M. and Gingeras,T.R. (2013) STAR: ultrafast universal RNA-seq aligner. *Bioinformatics*, **29**, 15–21.

30. Liao,Y., Smyth,G.K. and Shi,W. (2014) featureCounts: an efficient general purpose program for assigning sequence reads to genomic features. *Bioinformatics*, **30**, 923–930.

31. Love,M.I., Huber,W. and Anders,S. (2014) Moderated estimation of fold change and dispersion for RNA-seq data with DESeq2. *Genome Biol.*, **15**, 550.

32. Zhou,Y., Zhou,B., Pache,L., Chang,M., Khodabakhshi,A.H., Tanaseichuk,O., Benner,C. and Chanda,S.K. (2019) Metascape provides a biologist-oriented resource for the analysis of systems-level datasets. *Nat. Commun.*, **10**, 1523.

33. Raudvere,U., Kolberg,L., Kuzmin,I., Arak,T., Adler,P., Peterson,H. and Vilo,J. (2019) g:Profiler: a web server for functional enrichment analysis and conversions of gene lists (2019 update). *Nucleic Acids Res.*, **47**, W191–W198.

34. van Nuland,R., Smits,A.H., Pallaki,P., Jansen,P.W., Vermeulen,M. and Timmers,H.T. (2013) Quantitative dissection and stoichiometry determination of the human SET1/MLL histone methyltransferase complexes. *Mol. Cell. Biol.*, **33**, 2067–2077.

35. Luscher,B., Brizuela,L., Beach,D. and Eisenman,R.N. (1991) A role for the P34cdc2 kinase and phosphatases in the regulation of phosphorylation and disassembly of Lamin-B2 during the cell-cycle. *EMBO J.*, **10**, 865–875.

36. Gasek,N.S., Kuchel,G.A., Kirkland,J.L. and Xu,M. (2021) Strategies for targeting senescent cells in human disease. *Nat. Aging*, **1**, 870–879.

37. Schafer,M.J., White,T.A., Iijima,K., Haak,A.J., Ligresti,G., Atkinson,E.J., Oberg,A.L., Birch,J., Salmonowicz,H., Zhu,Y. *et al.* (2017) Cellular senescence mediates fibrotic pulmonary disease. *Nat. Commun.*, **8**, 14532.

38. Zhu,Y., Tchkonia,T., Pirtskhalava,T., Gower,A.C., Ding,H., Giorgadze,N., Palmer,A.K., Ikeno,Y., Hubbard,G.B., Lenburg,M. *et al.* (2015) The Achilles' heel of senescent cells: from transcriptome to senolytic drugs. *Aging Cell*, **14**, 644–658.

39. Bain,J., Plater,L., Elliott,M., Shpiro,N., Hastie,C.J., McLauchlan,H., Klevernic,I., Arthur,J.S., Alessi,D.R. and Cohen,P. (2007) The selectivity of protein kinase inhibitors: a further update. *Biochem. J.*, **408**, 297–315.

40. Folkes,A.J., Ahmadi,K., Alderton,W.K., Alix,S., Baker,S.J., Box,G., Chuckowree,I.S., Clarke,P.A., Depledge,P., Eccles,S.A. *et al.* (2008) The identification of 2-(1H-indazol-4-yl)-6-(4-methanesulfonyl-piperazin-1-ylmethyl)-4-morpholin-4-yl-t hieno(3,2-d)pyrimidine (GDC-0941) as a potent, selective, orally bioavailable inhibitor of class I PI3 kinase for the treatment of cancer. *J. Med. Chem.*, **51**, 5522–5532.

41. Anerillas,C., Abdelmohsen,K. and Gorospe,M. (2020) Regulation of senescence traits by MAPKs. *Geroscience*, **42**, 397–408.

42. Kuilman,T. and Peeper,D.S. (2009) Senescence-messaging secretome: SMS-ing cellular stress. *Nat. Rev. Cancer*, **9**, 81–94.

43. Gorgoulis,V., Adams,P.D., Alimonti,A., Bennett,D.C., Bischof,O., Bishop,C., Campisi,J., Collado,M., Evangelou,K., Ferbeyre,G. *et al.* (2019) Cellular senescence: defining a path forward. *Cell*, **179**, 813–827.

44. Lackner,D.H., Hayashi,M.T., Cesare,A.J. and Karlseder,J. (2014) A genomics approach identifies senescence-specific gene expression regulation. *Aging Cell*, **13**, 946–950.

45. Zirkel,A., Nikolic,M., Sofiadis,K., Mallm,J.P., Brackley,C.A., Gothe,H., Drechsel,O., Becker,C., Altmuller,J., Josipovic,N. *et al.* (2018) HMGB2 loss upon senescence entry disrupts genomic organization and induces CTCF clustering across cell types. *Mol. Cell*, **70**, 730–744.

46. Casella,G., Munk,R., Kim,K.M., Piao,Y., De,S., Abdelmohsen,K. and Gorospe,M. (2019) Transcriptome signature of cellular senescence. *Nucleic Acids Res.*, **47**, 7294–7305.

47. Jochems,F., Thijssen,B., De Conti,G., Jansen,R., Pogacar,Z., Groot,K., Wang,L., Schepers,A., Wang,C., Jin,H. *et al.* (2021) The cancer SENESCopedia: a delineation of cancer cell senescence. *Cell Rep.*, **36**, 109441.

48. Lee,S., Yu,Y., Trimpert,J., Benthani,F., Mairhofer,M., Richter-Pechanska,P., Wyler,E., Belenki,D., Kaltenbrunner,S., Pammer,M. *et al.* (2021) Virus-induced senescence is a driver and therapeutic target in COVID-19. *Nature*, **599**, 283–289.

49. Yang,Y.F., Pan,Y.H., Cao,Y., Fu,J., Yang,X., Zhang,M.F. and Tian,Q.H. (2017) PDZ binding kinase, regulated by FoxM1, enhances malignant phenotype via activation of beta-Catenin signaling in hepatocellular carcinoma. *Oncotarget*, **8**, 47195–47205.

50. Thiru,P., Kern,D.M., McKinley,K.L., Monda,J.K., Rago,F., Su,K.C., Tsinman,T., Yarar,D., Bell,G.W. and Cheeseman,I.M. (2014) Kinetochore genes are coordinately up-regulated in human tumors as part of a FoxM1-related cell division program. *Mol. Biol. Cell*, **25**, 1983–1994.

51. Wu,Z., Wang,Y.M., Dai,Y. and Chen,L.A. (2020) POLE2 serves as a prognostic biomarker and is associated with immune infiltration in squamous cell lung cancer. *Med. Sci. Monit.*, **26**, e921430.

52. Zhuang,J., Li,M., Zhang,X., Xian,S., Zhang,J., Yin,H., Liu,Y., Fan,M., Li,Z., Zhu,X. *et al.* (2022) Construction of bone metastasis-specific regulation network based on prognostic stemness-related signatures in prostate cancer. *Dis. Markers*, **2022**, 8495923.

53. Garcia-Muse,T. and Aguilera,A. (2016) Transcription-replication conflicts: how they occur and how they are resolved. *Nat. Rev. Mol. Cell Biol.*, **17**, 553–563.

54. Sharpless,N.E. and Sherr,C.J. (2015) Forging a signature of in vivo senescence. *Nat. Rev. Cancer*, **15**, 397–408.

55. Rogakou,E.P., Pilch,D.R., Orr,A.H., Ivanova,V.S. and Bonner,W.M. (1998) DNA double-stranded breaks induce histone H2AX phosphorylation on serine 139. *J. Biol. Chem.*, **273**, 5858–5868.

56. Burma,S., Chen,B.P., Murphy,M., Kurimasa,A. and Chen,D.J. (2001) ATM phosphorylates histone H2AX in response to DNA double-strand breaks. *J. Biol. Chem.*, **276**, 42462–42467.

57. Hernandez-Segura,A., de Jong,T.V., Melov,S., Guryev,V., Campisi,J. and Demaria,M. (2017) Unmasking transcriptional heterogeneity in senescent cells. *Curr. Biol.*, **27**, 2652–2660.

58. Shirakawa,J., Fernandez,M., Takatani,T., El Ouaamari,A., Jungtrakoon,P., Okawa,E.R., Zhang,W., Yi,P., Doria,A. and Kulkarni,R.N. (2017) Insulin signaling regulates the FoxM1/PLK1/CENP-A pathway to promote adaptive pancreatic beta cell proliferation. *Cell Metab.*, **25**, 868–882.

59. Wang,I.C., Chen,Y.J., Hughes,D., Petrovic,V., Major,M.L., Park,H.J., Tan,Y., Ackerson,T. and Costa,R.H. (2005) Forkhead box M1 regulates the transcriptional network of genes essential for mitotic progression and genes encoding the SCF (Skp2-Cks1) ubiquitin ligase. *Mol. Cell. Biol.*, **25**, 10875–10894.

60. Vaz,S., Ferreira,F.J., Macedo,J.C., Leor,G., Ben-David,U., Bessa,J. and Logarinho,E. (2021) FOXM1 repression increases mitotic death upon antimitotic chemotherapy through BMF upregulation. *Cell Death Dis.*, **12**, 542.

61. Cosentino,C. and Mostoslavsky,R. (2014) Sirtuin to the rescue: SIRT2 extends life span of BubR1 mice. *EMBO J.*, **33**, 1417–1419.

62. North,B.J., Rosenberg,M.A., Jeganathan,K.B., Hafner,A.V., Michan,S., Dai,J., Baker,D.J., Cen,Y., Wu,L.E., Sauve,A.A. *et al.* (2014) SIRT2 induces the checkpoint kinase BubR1 to increase lifespan. *EMBO J.*, **33**, 1438–1453.

63. Maehara,K., Takahashi,K. and Saitoh,S. (2010) CENP-A reduction induces a p53-dependent cellular senescence response to protect cells from executing defective mitoses. *Mol. Cell. Biol.*, **30**, 2090–2104.

64. Wang,X., Krupczak-Hollis,K., Tan,Y., Dennewitz,M.B., Adami,G.R. and Costa,R.H. (2002) Increased hepatic Forkhead Box M1B (FoxM1B) levels in old-aged mice stimulated liver regeneration through diminished p27Kip1 protein levels and increased Cdc25B expression. *J. Biol. Chem.*, **277**, 44310–44316.

65. Luscher-Firzlaff,J.M., Lilischkis,R. and Luscher,B. (2006) Regulation of the transcription factor FOXM1c by Cyclin E/CDK2. *FEBS Lett.*, **580**, 1716–1722.

66. Kalinichenko,V.V., Gusarova,G.A., Tan,Y., Wang,I.C., Major,M.L., Wang,X., Yoder,H.M. and Costa,R.H. (2003) Ubiquitous expression of the forkhead box M1B transgene accelerates proliferation of distinct pulmonary cell types following lung injury. *J. Biol. Chem.*, **278**, 37888–37894.

67. Sadasivam,S., Duan,S. and DeCaprio,J.A. (2012) The MuvB complex sequentially recruits B-Myb and FoxM1 to promote mitotic gene expression. *Genes Dev.*, **26**, 474–489.

68. Branigan,T.B., Kozono,D., Schade,A.E., Deraska,P., Rivas,H.G., Sambel,L., Reavis,H.D., Shapiro,G.I., D'Andrea,A.D. and DeCaprio,J.A. (2021) MMB-FOXM1-driven premature mitosis is required for CHK1 inhibitor sensitivity. *Cell Rep.*, **34**, 108808.

69. Lee,O.H., Woo,Y.M., Moon,S., Lee,J., Park,H., Jang,H., Park,Y.Y., Bae,S.K., Park,K.H., Heo,J.H. *et al.* (2020) Sirtuin 6 deficiency induces endothelial cell senescence via downregulation of forkhead box M1 expression. *Aging (Albany NY)*, **12**, 20946–20967.

70. Macedo,J.C., Vaz,S., Bakker,B., Ribeiro,R., Bakker,P.L., Escandell,J.M., Ferreira,M.G., Medema,R., Foijer,F. and Logarinho,E. (2018) FoxM1 repression during human aging leads to mitotic decline and aneuploidy-driven full senescence. *Nat. Commun.*, **9**, 2834.

71. Choi,Y.W., Nam,G.E., Kim,Y.H., Yoon,J.E., Park,J.H., Kim,J.H., Kang,S.Y. and Park,T.J. (2019) Abrogation of B-Raf(V600E) induced senescence by FoxM1 expression. *Biochem. Biophys. Res. Commun.*, **516**, 866–871.

72. Smirnov,A., Panatta,E., Lena,A., Castiglia,D., Di Daniele,N., Melino,G. and Candi,E. (2016) FOXM1 regulates proliferation, senescence and oxidative stress in keratinocytes and cancer cells. *Aging (Albany NY)*, **8**, 1384–1397.

73. Anders,L., Ke,N., Hydbring,P., Choi,Y.J., Widlund,H.R., Chick,J.M., Zhai,H., Vidal,M., Gygi,S.P., Braun,P. *et al.* (2011) A systematic screen for CDK4/6 substrates links FOXM1 phosphorylation to senescence suppression in cancer cells. *Cancer Cell*, **20**, 620–634.

74. Okuni,N., Honma,Y., Urano,T. and Tamura,K. (2022) Romidepsin and tamoxifen cooperatively induce senescence of pancreatic cancer cells through downregulation of FOXM1 expression and induction of reactive oxygen species/lipid peroxidation. *Mol. Biol. Rep.*, **49**, 3519–3529.

75. Jost,T., Heinzerling,L., Fietkau,R., Hecht,M. and Distel,L.V. (2021) Palbociclib induces senescence in melanoma and breast cancer cells and leads to additive growth arrest in combination with irradiation. *Front. Oncol.*, **11**, 740002.

76. Voong,C.K., Goodrich,J.A. and Kugel,J.F. (2021) Interactions of HMGB proteins with the genome and the impact on disease. *Biomolecules*, **11**, 1451.

77. Lawrence,I., Bene,M., Nacarelli,T., Azar,A., Cohen,J.Z., Torres,C., Johannes,G. and Sell,C. (2018) Correlations between age, functional status, and the senescence-associated proteins HMGB2 and p16(INK4a). *Geroscience*, **40**, 193–199.

78. Kimura,A., Matsuda,T., Sakai,A., Murao,N. and Nakashima,K. (2018) HMGB2 expression is associated with transition from a quiescent to an activated state of adult neural stem cells. *Dev. Dyn.*, **247**, 229–238.

79. Aird,K.M., Iwasaki,O., Kossenkov,A.V., Tanizawa,H., Fatkhutdinov,N., Bitler,B.G., Le,L., Alicea,G., Yang,T.L., Johnson,F.B. *et al.* (2016) HMGB2 orchestrates the chromatin landscape of senescence-associated secretory phenotype gene loci. *J. Cell Biol.*, **215**, 325–334.

80. Patel,A., Dharmarajan,V., Vought,V.E. and Cosgrove,M.S. (2009) On the mechanism of multiple lysine methylation by the human mixed lineage leukemia protein-1 (MLL1) core complex. *J. Biol. Chem.*, **284**, 24242–24256.

81. Southall,S.M., Wong,P.S., Odho,Z., Roe,S.M. and Wilson,J.R. (2009) Structural basis for the requirement of additional factors for MLL1 SET domain activity and recognition of epigenetic marks. *Mol. Cell*, **33**, 181–191.

82. Avdic,V., Zhang,P., Lanouette,S., Groulx,A., Tremblay,V., Brunzelle,J. and Couture,J.F. (2011) Structural and biochemical insights into MLL1 core complex assembly. *Structure*, **19**, 101–108.

83. Zhang,P., Chaturvedi,C.P., Tremblay,V., Cramet,M., Brunzelle,J.S., Skiniotis,G., Brand,M., Shilatifard,A. and Couture,J.F. (2015) A phosphorylation switch on RbBP5 regulates histone H3 Lys4 methylation. *Genes Dev.*, **29**, 123–128.

84. Steward,M.M., Lee,J.S., O'Donovan,A., Wyatt,M., Bernstein,B.E. and Shilatifard,A. (2006) Molecular regulation of H3K4 trimethylation by ASH2L, a shared subunit of MLL complexes. *Nat. Struct. Mol. Biol.*, **13**, 852–854.

85. Dou,Y., Milne,T.A., Ruthenburg,A.J., Lee,S., Lee,J.W., Verdine,G.L., Allis,C.D. and Roeder,R.G. (2006) Regulation of MLL1 H3K4 methyltransferase activity by its core components. *Nat. Struct. Mol. Biol.*, **13**, 713–719.

86. Eberl,H.C., Spruijt,C.G., Kelstrup,C.D., Vermeulen,M. and Mann,M. (2013) A map of general and specialized chromatin readers in mouse tissues generated by label-free interaction proteomics. *Mol. Cell*, **49**, 368–378.

87. Kim,J., Daniel,J., Espejo,A., Lake,A., Krishna,M., Xia,L., Zhang,Y. and Bedford,M.T. (2006) Tudor, MBT and chromo domains gauge the degree of lysine methylation. *EMBO Rep.*, **7**, 397–403.

88. Yun,M., Wu,J., Workman,J.L. and Li,B. (2011) Readers of histone modifications. *Cell Res.*, **21**, 564–578.

89. Morgan,M.A.J., Rickels,R.A., Collings,C.K., He,X., Cao,K., Herz,H.M., Cozzolino,K.A., Abshiru,N.A., Marshall,S.A., Rendleman,E.J. *et al.* (2017) A cryptic Tudor domain links BRWD2/PHIP to COMPASS-mediated histone H3K4 methylation. *Genes Dev.*, **31**, 2003–2014.

90. Patel,D.J. and Wang,Z. (2013) Readout of epigenetic modifications. *Annu. Rev. Biochem.*, **82**, 81–118.

91. Vermeulen,M., Mulder,K.W., Denissov,S., Pijnappel,W.W., van Schaik,F.M., Varier,R.A., Baltissen,M.P., Stunnenberg,H.G., Mann,M. and Timmers,H.T. (2007) Selective anchoring of TFIID to nucleosomes by trimethylation of histone H3 lysine 4. *Cell*, **131**, 58–69.

92. van Ingen,H., van Schaik,F.M., Wienk,H., Ballering,J., Rehmann,H., Dechesne,A.C., Kruijzer,J.A., Liskamp,R.M., Timmers,H.T. and Boelens,R. (2008) Structural insight into the recognition of the H3K4me3 mark by the TFIID subunit TAF3. *Structure*, **16**, 1245–1256.

93. Guccione,E., Bassi,C., Casadio,F., Martinato,F., Cesaroni,M., Schuchlautz,H., Luscher,B. and Amati,B. (2007) Methylation of histone H3R2 by PRMT6 and H3K4 by an MLL complex are mutually exclusive. *Nature*, **449**, 933–937.

94. Wysocka,J., Swigut,T., Xiao,H., Milne,T.A., Kwon,S.Y., Landry,J., Kauer,M., Tackett,A.J., Chait,B.T., Badenhorst,P. *et al.* (2006) A PHD finger of NURF couples histone H3 lysine 4 trimethylation with chromatin remodelling. *Nature*, **442**, 86–90.

95. Alkhatib,S.G. and Landry,J.W. (2011) The nucleosome remodeling factor. *FEBS Lett.*, **585**, 3197–3207.

96. Tallen,G. and Riabowol,K. (2014) Keep-ING balance: tumor suppression by epigenetic regulation. *FEBS Lett.*, **588**, 2728–2742.

97. Chung,H.R., Xu,C., Fuchs,A., Mund,A., Lange,M., Staege,H., Schubert,T., Bian,C., Dunkel,I., Eberharter,A. *et al.* (2016) PHF13 is a molecular reader and transcriptional co-regulator of H3K4me2/3. *Elife*, **5**, e10607.

98. Yang,Y., Augustin,J., Chang,C., Hu,J., Shah,K., Chang,C.W., Townes,T. and Jiang,H. (2014) The DPY30 subunit in SET1/MLL complexes regulates the proliferation and differentiation of hematopoietic progenitor cells. *Blood*, **124**, 2025–2033.

99. Malumbres,M. (2014) Cyclin-dependent kinases. *Genome Biol.*, **15**, 122.

100. Burgers,P.M.J. and Kunkel,T.A. (2017) Eukaryotic DNA Replication Fork. *Annu. Rev. Biochem*, **86**, 417–438.

101. Kirkland,J.L. and Tchkonia,T. (2017) Cellular senescence: a translational perspective. *EBioMedicine*, **21**, 21–28.

102. Tchkonia,T., Zhu,Y., van Deursen,J., Campisi,J. and Kirkland,J.L. (2013) Cellular senescence and the senescent secretory phenotype: therapeutic opportunities. *J. Clin. Invest.*, **123**, 966–972.

103. Lee,S. and Schmitt,C.A. (2019) The dynamic nature of senescence in cancer. *Nat. Cell Biol.*, **21**, 94–101.

104. Capell,B.C., Drake,A.M., Zhu,J., Shah,P.P., Dou,Z., Dorsey,J., Simola,D.F., Donahue,G., Sammons,M., Rai,T.S. *et al.* (2016) MLL1 is essential for the senescence-associated secretory phenotype. *Genes Dev.*, **30**, 321–336.

105. Haq,R., Brenton,J.D., Takahashi,M., Finan,D., Finkielsztein,A., Damaraju,S., Rottapel,R. and Zanke,B. (2002) Constitutive p38HOG mitogen-activated protein kinase activation induces permanent cell cycle arrest and senescence. *Cancer Res.*, **62**, 5076–5082.

106. Wang,W., Chen,J.X., Liao,R., Deng,Q., Zhou,J.J., Huang,S. and Sun,P. (2002) Sequential activation of the MEK-extracellular signal-regulated kinase and MKK3/6-p38 mitogen-activated protein kinase pathways mediates oncogenic ras-induced premature senescence. *Mol. Cell. Biol.*, **22**, 3389–3403.

107. Freund,A., Patil,C.K. and Campisi,J. (2011) p38MAPK is a novel DNA damage response-independent regulator of the senescence-associated secretory phenotype. *EMBO J.*, **30**, 1536–1548.

108. Slobodnyuk,K., Radic,N., Ivanova,S., Llado,A., Trempolec,N., Zorzano,A. and Nebreda,A.R. (2019) Autophagy-induced senescence is regulated by p38alpha signaling. *Cell Death. Dis.*, **10**, 376.

109. Baar,M.P., Brandt,R.M.C., Putavet,D.A., Klein,J.D.D., Derks,K.W.J., Bourgeois,B.R.M., Stryeck,S., Rijksen,Y., van Willigenburg,H., Feijtel,D.A. *et al.* (2017) Targeted apoptosis of senescent cells restores tissue homeostasis in response to chemotoxicity and aging. *Cell*, **169**, 132–147.

110. Greuber,E.K., Smith-Pearson,P., Wang,J. and Pendergast,A.M. (2013) Role of ABL family kinases in cancer: from leukaemia to solid tumours. *Nat. Rev. Cancer*, **13**, 559–571.

111. Reis,A. and Hermanson,O. (2012) The DNA glycosylases OGG1 and NEIL3 influence differentiation potential, proliferation, and senescence-associated signs in neural stem cells. *Biochem. Biophys. Res. Commun.*, **423**, 621–626.

112. Zhao,Z., Gad,H., Benitez-Buelga,C., Sanjiv,K., Xiangwei,H., Kang,H., Feng,M., Zhao,Z., Berglund,U.W., Xia,Q. *et al.* (2021) NEIL3 prevents senescence in hepatocellular carcinoma by repairing oxidative lesions at telomeres during mitosis. *Cancer Res.*, **81**, 4079–4093.

113. Meyer,C., Burmeister,T., Groger,D., Tsaur,G., Fechina,L., Renneville,A., Sutton,R., Venn,N.C., Emerenciano,M., Pombo-de-Oliveira,M.S. *et al.* (2018) The MLL recombinome of acute leukemias in 2017. *Leukemia*, **32**, 273–284.

114. Takacova,S., Slany,R., Bartkova,J., Stranecky,V., Dolezel,P., Luzna,P., Bartek,J. and Divoky,V. (2012) DNA damage response and inflammatory signaling limit the MLL-ENL-induced leukemogenesis in vivo. *Cancer Cell*, **21**, 517–531.

115. Tajima,K., Matsuda,S., Yae,T., Drapkin,B.J., Morris,R., Boukhali,M., Niederhoffer,K., Comaills,V., Dubash,T., Nieman,L. *et al.* (2019) SETD1A protects from senescence through regulation of the mitotic gene expression program. *Nat. Commun.*, **10**, 2854.

116. Shimoda,H., Doi,S., Nakashima,A., Sasaki,K., Doi,T. and Masaki,T. (2019) Inhibition of the H3K4 methyltransferase MLL1/WDR5 complex attenuates renal senescence in ischemia reperfusion mice by reduction of p16(INK4a). *Kidney Int.*, **96**, 1162–1175.

117. Simboeck,E., Gutierrez,A., Cozzuto,L., Beringer,M., Caizzi,L., Keyes,W.M. and Di Croce,L. (2013) DPY30 regulates pathways in cellular senescence through ID protein expression. *EMBO J.*, **32**, 2217–2230.